Received: 5 June 2023 | Revised: 25 September 2023 | Accepted: 25 September 2023

DOI: 10.1002/rcm.9650

PROTOCOL

Rapid Communications in Mass Spectrometry WILEY

Analytical improvements and assessment of long-term performance of the oxidation–denitrifier method

Simone Moretti[1,2] | Nicolas N. Duprey[1] | Alan D. Foreman[1] | Anthea Arns[1] | Sven Brömme[1] | Jonathan Jung[1] | Xuyuan E. Ai[1,3] | Alexandra Auderset[1,4] | Aaron L. Bieler[1] | Camino Eck[1] | Jesse Farmer[1,3,5] | Barbara Hinnenberg[1] | Matthew Lacerra[1,3] | Jennifer Leichliter[1] | Tina Lüdecke[1] | Sergey Oleynik[3] | Florian Rubach[1] | Mareike Schmitt[1] | Marissa Vink[1] | Tanja Wald[1] | Maayan Yehudai[1] | Daniel M. Sigman[3] | Alfredo Martínez-García[1]

[1]Climate Geochemistry Department, Max Planck Institute for Chemistry, Hahn-Meitner-Weg 1, Mainz, 55128, Germany

[2]Istituto di Scienze Polari, Consiglio Nazionale delle Ricerche, Via Piero Gobetti 101, Bologna, 40129, Italy

[3]Department of Geosciences, Princeton University, Princeton, New Jersey, USA

[4]Ocean and Earth Science Programme, University of Southampton, Southampton, UK

[5]School for the Environment, University of Massachusetts Boston, Boston, Massachusetts, USA

Correspondence
S. Moretti, Climate Geochemistry Department, Max Planck Institute for Chemistry, Mainz, Germany.
Email: simone.moretti@mpic.de

A. Martínez-García, Climate Geochemistry Department, Max Planck Institute for Chemistry, Mainz, Germany.
Email: a.martinez-garcia@mpic.de

Funding information
Deutsche Forschungsgemeinschaft, Grant/Award Number: 468591845 - SPP 2299/Project number 44183248; Emmy Noether Fellowship, Grant/Award Number: LU 2199/2-1; Max-Planck-Gesellschaft; The Paul Crutzen Nobel Prize Fellowship

The analysis of the nitrogen (N) isotopic composition of organic matter bound to fossil biomineral structures (BB-$\delta^{15}N$) using the oxidation–denitrifier (O–D) method provides a novel tool to study past changes in N cycling processes.

Methods: We report a set of methodological improvements to the O–D method, including (a) a method for sealing the reaction vials in which the oxidation of organic N to NO_3^- takes place, (b) a recipe for bypassing the pH adjustment step before the bacterial conversion of NO_3^- to N_2O, and (c) a method for storing recrystallized dipotassium peroxodisulfate ($K_2S_2O_8$) under Ar atmosphere.

Results: The new sealing method eliminates the occasional contamination and vial breakage that occurred previously while increasing sample throughput. The protocol for bypassing pH adjustment does not affect BB-$\delta^{15}N$, and it significantly reduces the processing time. Storage of $K_2S_2O_8$ reagent under Ar atmosphere produces stable oxidation blanks over more than 3.5 years. We report analytical blanks, accuracy, and precision for this methodology from eight users over the course of ~3.5 years of analyses at the Max Planck Institute for Chemistry. Our method produces analytical blanks characterized by low N content (0.30 ± 0.13 nmol N, 1σ, $n = 195$) and stable $\delta^{15}N$ (−2.20 ± 3.13‰, $n = 195$). The analysis of reference amino acid standards USGS 40 and USGS 65 indicates an overall accuracy of −0.23 ± 0.35‰ (1σ, $n = 891$). The analysis of in-house fossil standards gives similar analytical precision (1σ) across a range of BB-$\delta^{15}N$ values and biominerals: zooxanthellate coral standard PO-1 (6.08 ± 0.21‰, $n = 267$), azooxanthellate coral standard LO-1 (10.20 ± 0.28‰, $n = 258$), foraminifera standard MF-1 (5.92 ± 0.28‰, $n = 243$), and tooth enamel AG-Lox (4.06 ± 0.49‰, $n = 78$).

Simone Moretti, Nicolas N. Duprey, and Alan D. Foreman contributed equally to this study.

Conclusions: The methodological improvements significantly increase sample throughput without compromising analytical precision or accuracy down to 1 nmol of N.

1 | INTRODUCTION

The natural variation in the ratio of the nitrogen isotopes (i.e., the $^{15}N/^{14}N$ ratio) has been used extensively over the past decades to trace a vast array of biologically mediated transformations of this element in modern terrestrial and marine environments.[1–5] Despite an early recognition of the potential utility of N isotopes for elucidating past changes in both the N cycle and past food webs, their application to the fossil record was initially hindered by the low concentrations of organic N typically found in biominerals (typically 1–10 nmol/mg). This range of concentrations imposed an analytical barrier for the analysis of biominerals using conventional measurement techniques (e.g., elemental analyzer [EA] coupled to isotope ratio mass spectrometry [IRMS]), which normally have required sample sizes in the micromole range.[6,7]

The advent of the denitrifier method in 2001 first allowed for analysis of the nitrogen and oxygen isotopic composition (hereafter $\delta^{15}N$ and $\delta^{18}O$, where $\delta^{15}N = [((^{15}N/^{14}N)_{sample} / (^{15}N/^{14}N)_{atm\ N2}) - 1) \times 1000]$ and $\delta^{18}O = [((^{18}O/^{16}O)_{sample} / (^{18}O/^{16}O)_{VSMOW}) - 1) \times 1000]$) of seawater and freshwater NO_3^- at nmol concentrations.[8,9] Briefly, the denitrifier method relies on the use of denitrifying bacteria that lack nitrous oxide reductase activity, *Pseudomonas chlororaphis* (ATCC# 43928, Manassas, VA, USA) and *P. chlororaphis* subsp. *aureofaciens* (ATCC# 13985, Manassas, VA, USA),[10] to quantitatively convert NO_3^- to N_2O. Bacterially produced N_2O is purified and concentrated with a custom-built system and delivered to an IRMS. This method allows for the precise and accurate determination of the $\delta^{15}N$ of NO_3^- down to 1–2 nmol of N. For an in-depth discussion of the bacterial preparation, the conversion of NO_3^- to N_2O, and its subsequent measurement, the reader is redirected to literature.[8,9,11,12]

The precision and accuracy of the denitrifier method at nanomole concentrations prompted a recognition that, by pairing it with an oxidation method that converts organic matter and other reduced N forms to nitrate,[13,14] the N isotope composition of organic matter preserved in biominerals could be constrained.[15] Specifically, these authors demonstrated that, by coupling the products of a dipotassium peroxodisulfate ($K_2S_2O_8$) oxidation reaction, first developed by Nydahl,[16] to convert dissolved organic N species to NO_3^-, with the denitrifier method described by Sigman et al.,[9] they could achieve accurate and precise analysis of the $\delta^{15}N$ of reduced forms of N at nanomolar quantities.[14]

This coupled oxidation–denitrifier (O–D) method thus provided a platform by which the precise analysis of the N isotopic composition of organic N bound in various fossil and modern biogenic minerals could be achieved. With the increasing recognition that the $\delta^{15}N$ of the organic matter enclosed within biominerals is diagenetically robust and reflects the isotopic composition of the host organism's N, the biomineral-bound N isotopes or BB-$\delta^{15}N$ has been applied to a variety of archives over the past two decades, including foraminifera,[17–31] deep- and shallow-water scleractinian corals,[32–44] tooth enamel/enameloid,[45–48] fish otoliths,[49–51] and diatoms.[58,59]

The substantial increase in the applications of the O–D method has raised the need for procedural improvements to increase sample throughput without losing precision or accuracy. Here, we report modifications to the method aimed at overcoming three previous difficulties. First, in the original method, each dissolved sample was combined with the basic $K_2S_2O_8$ oxidative reagent in a precombusted borosilicate glass vial closed with a Teflon-lined cap; these vials were prone to leakage, contamination, and/or breakage. Second, following the oxidation step, the high pH of the sample solution (13-14) required the samples to be acidified before their injection into the denitrifying bacteria to avoid disruption of bacterial physiology. This process is sample specific and time consuming. Last, best practices for storing the recrystallized $K_2S_2O_8$ reagent to minimize its contribution to the oxidation blank have remained an open question, with approaches varying among users and laboratories. The analytical improvements to the O–D method described here address these problems and have allowed us to increase our sample throughput without compromising analytical precision (Figure 1). We evaluate the long-term interuser reproducibility of this updated methodology and its performance over a range of 1–20 nmol of N over 3 years of observations at the Max Planck Institute for Chemistry (MPIC).

2 | EXPERIMENTAL

2.1 | Analytical improvements to the oxidation-denitrifier method

The general methodology used in this study is based on the O–D methods developed for the analysis of foraminifera,[26] stony corals,[40] and tooth enamel[47] samples. All consumables and equipment used for the experiments listed are provided in Tables S1 and S2 (supporting information). To optimize the sample throughput, three modifications were introduced:

1. *Vial rack for the oxidation step ("sandwich").* The standard phenolic caps used to seal the 4 mL borosilicate glass vials for the oxidation step by Knapp et al[14] were the only off-shelf product able to maintain adequate sealing over an autoclave cycle (120°C) and have been a crucial consumable used in this method over the past two decades. These caps come with a major drawback, however, as the phenolic material tends to degrade quickly when exposed to

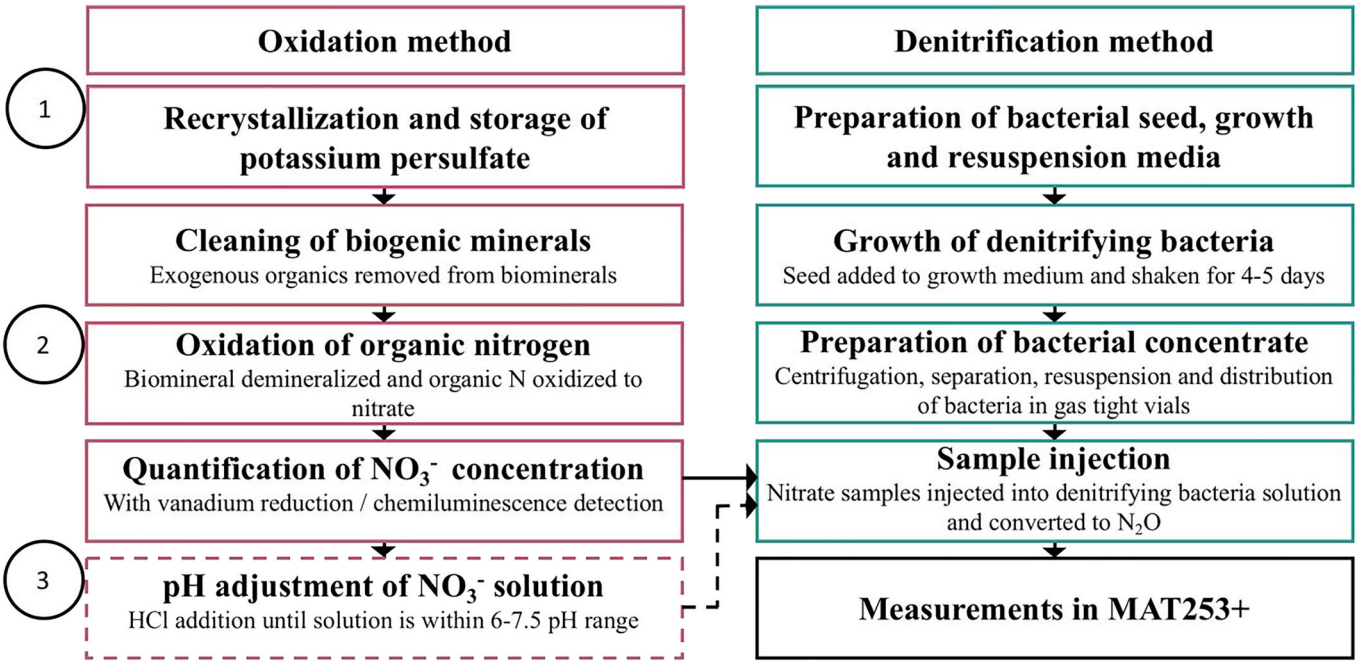

FIGURE 1 Summary of the steps of oxidation–denitrifier (O–D) method. The steps are summarized sequentially for both the oxidation (red) and denitrifier methods (green). Side arrows connect steps that are co-occurring between the oxidation and the denitrification parts of the method. The preparation of bacterial seed, growth, and resuspension media and the preparation of bacterial concentrate and injections (green) are discussed extensively in Weigand et al.[12] Numbered circles refer to the methodological improvements discussed in this work. The dashed outline on the pH adjustment box refers to methodological improvements discussed in this work that allow to bypass pH adjustment of the NO_3^- solutions amended to denitrifying bacteria (Section 2.1). [Color figure can be viewed at wileyonlinelibrary.com]

heat and water, becoming brittle and potentially leaching out N-containing compounds. To prevent contamination, a thin rubber liner coated with polytetrafluoroethylene (PTFE) is fit inside each cap. Contamination of samples occurs sporadically when these caps are used, which can be identified by their anomalously high N content, although the possibility of lower-level contamination across a greater number of samples is more difficult to assess. The addition of an extra oxidatively cleaned PTFE liner between the cap and the sample vial significantly decreased the number of contaminated samples but did not completely eliminate their occurrence.

In addition, single-use phenolic caps required substantial pretreatment before sample oxidation. Each cap first had to be prerinsed with milliQ water and dried, and the single-use precut PTFE liners had to be oxidized with a solution of $K_2S_2O_8$ and NaOH, rinsed with milliQ water, and dried. Finally, the two had to be manually assembled by each user before oxidation.

To reduce occasional contamination from the phenolic caps and increase sample throughput, we designed a rack in which the vials are placed open in an aluminum holder and closed by a single-use 0.1 mm PTFE sheet and a reusable 3 mm silicone mat (Figure 2). The rack is then "sandwiched" between two 14 mm-thick aluminum plates and held in place with bolts and nuts to seal the PTFE and silicone layers atop the oxidation vials, thereby preventing leaks and atmospheric contamination (Figure S1 [supporting information]). The bolt-

FIGURE 2 Experimental setup for sealing reaction vials during the oxidative conversion of organic nitrogen to nitrate. To seal vials during conversion, up to 120 vials are placed in an aluminum rack and covered with a 0.1 mm–thick Teflon sheet followed by a silicon mat. This stack is squeezed between two aluminum plates by means of threaded bolts to provide a good seal on all vials simultaneously. This setup substitutes the previously used phenolic caps that were manually lined with 0.1 mm polytetrafluoroethylene septa. By making use of easily accessible materials, it represents a cost-effective setup that reduces consumables costs and increases sample throughput. [Color figure can be viewed at wileyonlinelibrary.com]

tightening torque is on the order of 7 N·m, ensuring a tight seal throughout the whole area of the assembly. Adequate sealing can be achieved by tightening the bolts with a manual wrench or via a small battery-powered drill. Testing revealed no significant difference in blank size or reference material (RM) $\delta^{15}N$ with respect to the position of the vials in the rack, suggesting an even distribution

sealing capacity (Figure S2 [supporting information]). This design allows the oxidation step to proceed without the need for phenolic caps. After the autoclaving, vials can be capped with regular polypropylene caps, as organic contaminants are no longer an issue once the oxidation reaction to NO_3^- has taken place and the reagent is exhausted. This new method for sealing the reaction vials eliminates the occasional contamination of samples from vial caps and increases the number of samples that can be oxidized in one sample batch (120 vials per current methodology), without compromising analytical precision or accuracy (see Section 3). We provide a full 3D model of the assembly in STEP format in the supporting information.

2. *Bypassing the pH balancing step*. The need for the oxidizing solution to remain basic during the autoclave step[16] means that each oxidized sample has an elevated pH (13–14) that could potentially alter bacterial physiology if injected without acidification. Previously, sample acidification was carried out by iterative incremental addition of small (1–5 µL) amounts of 4 M hydrochloric acid (HCl) to the solution. After each addition, the pH of the sample was tested by manually transferring a small amount (~15 µL) of the sample solution to a pH strip. In case of excessive addition of HCl, the pH had to be elevated back to physiological values via the addition of 2 M NaOH. This step is time consuming (e.g., 5–8 h for 80 samples) and can lead to the consumption of up to 10% of the sample solution during pH testing. Previously, both the 4 M HCl solution used to dissolve the biomineral sample and the NaOH solution were made on the day of the oxidative step from an ultrahigh purity (Fisher Optima grade) 12 M HCl mother stock and NaOH pellets, respectively, to minimize contamination. This added further time requirements for the pH-balancing step. Below, we describe updates to the method aimed at bypassing the pH balancing by (a) standardizing the amount of NaOH added during the oxidation step and (b) optimizing the buffer capacity of the bacterial medium.

The first of these is aimed at standardizing the preparation of the "persulfate oxidizing reagent" (POR) solution used in the oxidation step.[14,26] We do so to constrain and minimize the amount of excess NaOH (the amount of residual NaOH in a sample) in solution after the oxidation, while still ensuring that enough NaOH remains to compensate for the protons generated during the decomposition of the $K_2S_2O_8$.[16] We achieved standardization of the POR solution by preparing batches of single-use 10 mL aliquots of 4 M HCl for mineral dissolution and batches of single-use 10 mL aliquots of concentrated NaOH solution for preparing the high-pH POR solution. The 4 M HCl aliquots were prepared by diluting a mother solution of 12 M HCl (Table S1 [supporting information]). The aliquots of 4 M HCl were stored in 12 mL precombusted borosilicate glass vials at −20°C. A constant amount of 45 µL of this 4 M HCl is added to each sample for demineralization, so a single 10 mL vial is enough to dissolve an entire sample batch of 80 samples (5–8 mg $CaCO_3$) and 20 standards. The NaOH solution for the POR was prepared at a concentration of 6.25 M and split into 10 mL single-use aliquots kept in 15 mL polypropylene tubes stored at −20°C. A fixed volume of 4 mL of this 6.25 M NaOH solution was taken from the single-use aliquot and mixed with 96 mL of milliQ water. Finally, 0.7 g of recrystallized $K_2S_2O_8$ was added to that mixture (Table S1 [supporting information]). One milliliter of POR was amended into each sample, and vials were sealed using the new vial rack and placed in the autoclave at 120°C for 65 min. The use of premade single-use aliquots of HCl and NaOH for sample acidification and preparation of the POR significantly reduces inter- and intrauser variability and reduces processing times.

The second improvement involves enhancing the buffering capacity of the *P. chlororaphis* resuspension media used in the denitrifier method so that more than 60 ± 4 µmol of NaOH can be added without increasing the pH beyond the upper range of the bacterial optimum, that is, pH 7.5.[60] For this purpose, we used a resuspension media recipe buffered at pH 6.3 made with potassium phosphate monobasic (KH_2PO_4), instead of potassium phosphate dibasic (K_2HPO_4); the pH 6.3 media recipe has been used previously for coupled nitrate N and O isotope measurements using the *P. chlororaphis* subsp. *aureofaciens* strain.[8,12] In addition to changing the recipe, we tested whether using more resuspension media per headspace vial (3 mL) than previous studies (1 to 1.5 mL[12,26,40]) had an impact on the precision and accuracy of the results; a larger volume of buffered resuspension media provides an increased buffering capacity per bacterial vial.

To constrain the altered buffering capacity of the new resuspension media recipe and the impact of the increased volume of resuspension media per headspace vial, we measured the pH of freshly harvested *P. chlororaphis* bacteria resuspended in the media with pH 6.3 injected with between 0 and 1000 µL of non-pH-adjusted oxidized solutions with varying excess NaOH concentration (Section 3.1). The oxidized solutions contained 0 (oxidation blanks and amino acid standards), 2, 4, and 8 mg of the in-house coral standard PO-1 (Table S3 [supporting information]). The oxidation, the bacterial harvest, the bacteria resuspension, and the injection to the headspace vials were carried out following the same protocol used for coral samples.[12,42]

3. *Recrystallized $K_2S_2O_8$ storage*. The highly oxidative properties of $K_2S_2O_8$ mean that it is likely to convert any form of reactive N present in the laboratory environment to NO_3^-. As such, it has the potential to contribute substantially to oxidation blanks in the O–D method given its essential role in the oxidation step and its tendency to bear significant N.[16] To address this issue, off-shelf reagent-grade $K_2S_2O_8$ is typically recrystallized four times before use to reduce oxidation blanks[14] (see supporting information for recrystallization protocol). This process is time consuming, and, although the recrystallized $K_2S_2O_8$ is typically stored in a desiccator, past users have reported that oxidation blanks tend to increase within weeks after recrystallization. Therefore, freshly recrystallized $K_2S_2O_8$ is typically used only for a maximum of 3 months after recrystallization.

To improve the useful lifetime of the recrystallized $K_2S_2O_8$ reagent, we tested the storage of freshly recrystallized $K_2S_2O_8$ in 0.8–1 g aliquots under argon (Ar) atmosphere in 20 mL EPA glass vials vacuum-sealed inside an aluminum-coated bag. Each aliquot is used only once to minimize the exposure of the clean reagent to lab air and moisture. In Figure S3 (supporting information), we provide a full 3D model of the apparatus used in STEP format to replace the atmosphere in the EPA vials with Ar.

The three changes described earlier represent a substantial improvement in sample throughput for the O–D method, but whether any of them alter the precision or accuracy of the O–D method remains an open question. To evaluate the potential impact of the changes in the O–D method described earlier, eight individual users reported $\delta^{15}N$ and N content measurements of oxidation blanks, international RM (also called standard) amino acids, and in-house biomineral RMs over ~3.5 years.

2.2 | Data correction and estimation of accuracy and precision

Conversion of $\delta^{15}N$ IRMS data from the denitrifier method to an international RM (vs. air) is a two-step process. First, N_2O measurements are normalized against an N_2O tank that is analyzed in parallel to sample N_2O for each sample. Second, they are normalized to air on a true-versus-analyzed $\delta^{15}N$ scale using two potassium nitrate standards: USGS 34 (The National Institute of Standards and Technology, Gaithersburg, MD, USA [−1.8 ± 0.2‰]) and IAEA-NO3 (International Atomic Energy Agency, Vienna, Austria [+4.7 ± 0.2‰]).[61] Although this normalization accounts for offsets introduced during measurement and the denitrifier step of the method, it does not take into account blanks introduced during the oxidation step.

To solve this problem, the N content and $\delta^{15}N$ of the blank from the oxidation step onward are measured directly and subtracted from each individual measurement using a simple two end-member mixing model. Although the measurement of the isotopic composition of the blank in a single vial is not possible due to the extremely low N content of oxidation blanks (~0.3 nmol; see Section 3.2), it can be achieved by combining four to five individual 1-mL oxidation blanks to achieve a combined blank size of 1 to 2 nmol of N. N contents in this range (1–3 nmol) require additional empirical correction due to a combination of shot noise and an increase in the relative fraction of bacterial N introduced to the sample.[12] The combined blank measurement was thus corrected by quantifying the offset from the true value of USGS 34 and IAEA-NO3 in the size range of oxidation blanks (from 0.5 to 3 nmol; Figure S4 [supporting information]) and removing this offset from the blank $\delta^{15}N$ measurements. The N content and $\delta^{15}N$ of the blank ($\delta^{15}N_{blank}$) were then incorporated in a two end-member mixing model correction that takes into account the fraction of the blank (F_{blank}) and $\delta^{15}N$ measured for each sample ($\delta^{15}N_{measured}$). This correction was applied to all oxidized samples and RMs to estimate the blank-corrected $\delta^{15}N$ value ($\delta^{15}N_{sample}$):

$$\delta^{15}N_{measured} = \delta^{15}N_{sample}(1 - F_{blank}) + \delta^{15}N_{blank} \cdot F_{blank}$$

To estimate the accuracy and precision of the modified O–D method we presented in Section 2.1, we used international RM amino acids USGS 40 and 65 (Table S3 [supporting information]) measured in each sample batch. It is essential to note that, unlike other studies,[24,26,29,41] in this work these amino acid RMs were not used for blank $\delta^{15}N$ estimation and, therefore, can be used to independently monitor the accuracy and precision of the method from the oxidation step onward.

To date, a method to directly measure the full procedural blank, that is, accounting for both the oxidation blank and the potential contribution of the biomineral cleaning step, is lacking. This is because the quantification of such a contribution would require a representative biomineral with no N content. Such material is not easily obtainable; in-house testing reveals that even abiotic carbonates have a small but significant amount of residual N. In-house experiments at the MPIC attempted to artificially create N-free material by heating different biomineral powders at 100–500°C; however, these experiments were unable to completely remove all organic N without destroying the biomineral matrix.[62] Thus, the long-term precision of the complete O–D method, as well as the potential contribution of any procedural blank introduced during the cleaning step, was quantified using in-house biomineral RMs that were cleaned and analyzed in each sample batch (Table S3 [supporting information]).

3 | RESULTS AND DISCUSSION

In this section, we describe $\delta^{15}N$ and N content results of analyses of international and in-house RMs from eight users over the span of 3.5 years and evaluate the precision and accuracy of the O–D method using the changes described earlier. We begin by describing the buffering characteristics of the altered resuspension media and demonstrate that the addition of nonacidified samples to this new media provides results that are statistically indistinguishable from acidified (i.e., "pH-balanced") samples (Section 3.1). Next, we show that the oxidation blanks produced using the adapted O–D method are both stable and consistently low across the entire measurement period (Section 3.2) across eight users. We demonstrate that the changes in the storage method of $K_2S_2O_8$ produce blanks that are consistent and stable over the entire 2.5-year period that we tested (Section 3.2). Last, we evaluate the long-term accuracy and precision of international RMs (Section 3.3) and in-house biomineral RMs (Section 3.4) and demonstrate that we can achieve methodological precision down to 1 nmol of N (Section 3.5).

3.1 | Bypassing pH adjustment

The oxidations described in this and any following sections were performed using the apparatus detailed in Section 2.1 and Figure 1.

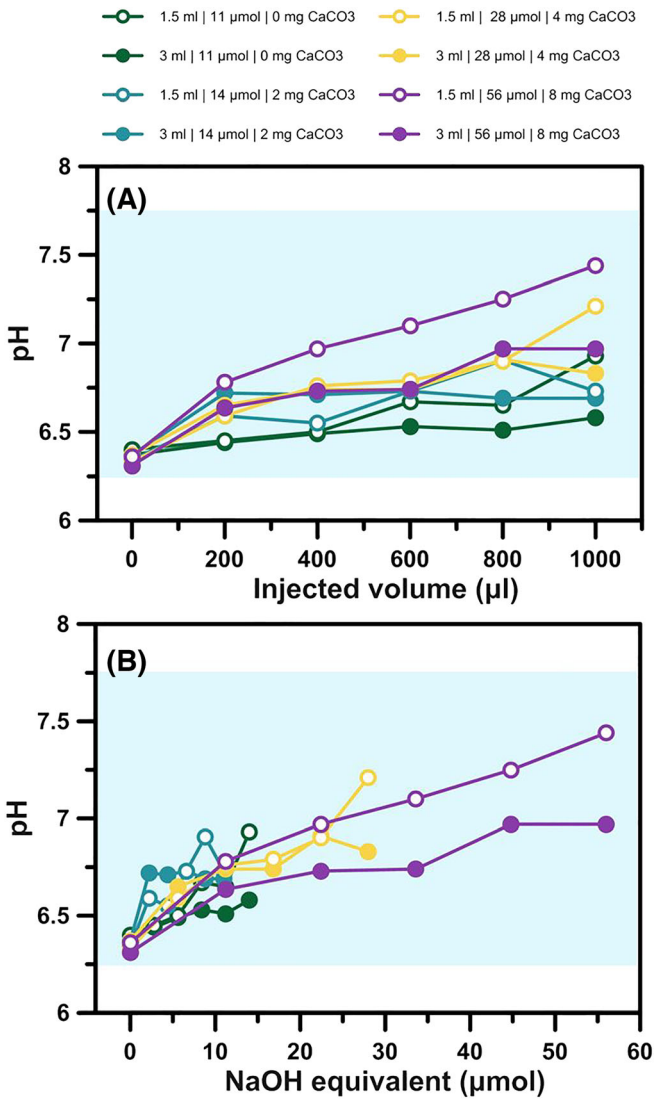

FIGURE 3 Testing the pH buffering capacity of freshly harvested *Pseudomonas chlororaphis*. A, potassium phosphate monobasic pH change of the solution inside the headspace vial after sample amendment of different amounts of persulfate oxidizing reagent–oxidized solution. The impact of four different carbonate sample sizes (0, 2, 4, and 8 mg) corresponding to four equivalent excess NaOH injection amounts (11, 14, 28, and 56 µmol, respectively) using two different volumes of bacteria resuspension media: 1.5 mL (open symbols) and 3 mL (closed symbols). B, Same dataset plotted against the corresponding injected excess NaOH content. Blue shading represents the typical physiological pH range for *P. chlororaphis*. [Color figure can be viewed at wileyonlinelibrary.com]

As described in Section 2.1, we evaluated the buffering capacity of the bacteria resuspension media to determine the range in sample size that could be added to a bacterial vial without the need for pH adjustment. About 1000 µL of the sample solution with 0 (oxidation blank), 2, 4, and 8 mg of dissolved and oxidized coral samples had an equivalent of 11, 14, 28, and 56 µmol of excess NaOH, respectively. Adding each of these to 3 mL of bacteria resuspension media buffered at pH 6.3 resulted in the following pH changes: 6.58, 6.69, 6.83, and 6.97. This range of pH is well within the optimal pH range reported for *P. chlororaphis* (pH 6.3–7.5; Figure 3A), meaning that optimal conditions for full conversion of the sample NO_3^- into N_2O can be achieved across a wide range of sample sizes. It is worth noting that, in previous studies, the bacteria cultures were resuspended in media buffered at pH 7.3 for *P. chlororaphis*,[12] a value higher than the highest value reported in this experiment (pH 6.97).

We repeated the experiment using 1.5 mL of resuspension media instead of 3 mL, to simulate more extreme scenarios with regard to sample size. The highest amount of NaOH (i.e., 56 µmol of excess NaOH, associated with 8 mg of coral powder) amended to 1.5 mL of resuspension media resulted in a pH of 7.44 (Figure 3B), which is still lower than the upper pH range for *P. chlororaphis* pH optimum, highlighting the large buffering capacity of the media used. We chose to routinely use 2.75 to 3 mL of resuspension media for each sample for experiments spanning the past 3.5 years to ensure a higher buffering capacity. The higher bacterial media-to-sample volume ratio has the additional benefit of minimizing the local loss of bacteria upon sample injection before homogenization of the vial by shaking.

We next evaluated whether bypassing the pH adjustment led to significant differences in sample $\delta^{15}N$ and weight-normalized N content values relative to the previous protocol that included pH adjustment.[14] For this test we processed two in-house calcium carbonate ($CaCO_3$) coral RMs (PO-1, LO-1), one international amino acid RM (USGS 40), and a set of scleractinian coral samples (*Pocillopora damicornis*). For all materials, each sample was analyzed twice in the same batch, one with pH adjustment and one without.

A cross-plot of the results obtained with the two methodologies yields a regression line that is statistically undistinguishable (95% confidence envelope) from a theoretical 1:1 line (Figure 4A), suggesting no difference for both $\delta^{15}N$ and weight-normalized N content in all samples and RM types. The median of the differences between the paired samples for each treatment was always <0.2‰ for $\delta^{15}N$ and <0.1 nmol/mg for weight-normalized N content (Figure 4B and Table 1). A two-tailed unpaired *t*-test ($\alpha < 0.05$) between whole dataset means of paired pH-adjusted and non-pH-adjusted amino acids, PO-1 and LO-1 RMs, and coral samples (Table 1) further shows no statistically significant difference between methods ($p > 0.05$ in all cases). These results demonstrate that bypassing the pH adjustment does not result in a statistically significant offset in either $\delta^{15}N$ or weight-normalized N content with respect to samples processed with the former method. We, therefore, conclude that oxidized NO_3^- samples can be injected directly into denitrifying bacteria using 2.75 to 3 mL of resuspended bacteria media buffered with KH_2PO_4. Although this requires a larger amount of bacteria solution per sample, bypassing the pH adjustment step simplifies the procedure and significantly reduces laboratory time (by as much as 5–8 h, depending on the batch size). All RM data (amino acid and biomineral) presented in the following sections were obtained by injection into bacteria bypassing the pH-balancing step, as described earlier. Although it is likely that oxidation blanks could also be injected directly into the bacteria, we chose to acidify these samples because they require the combination of five individual

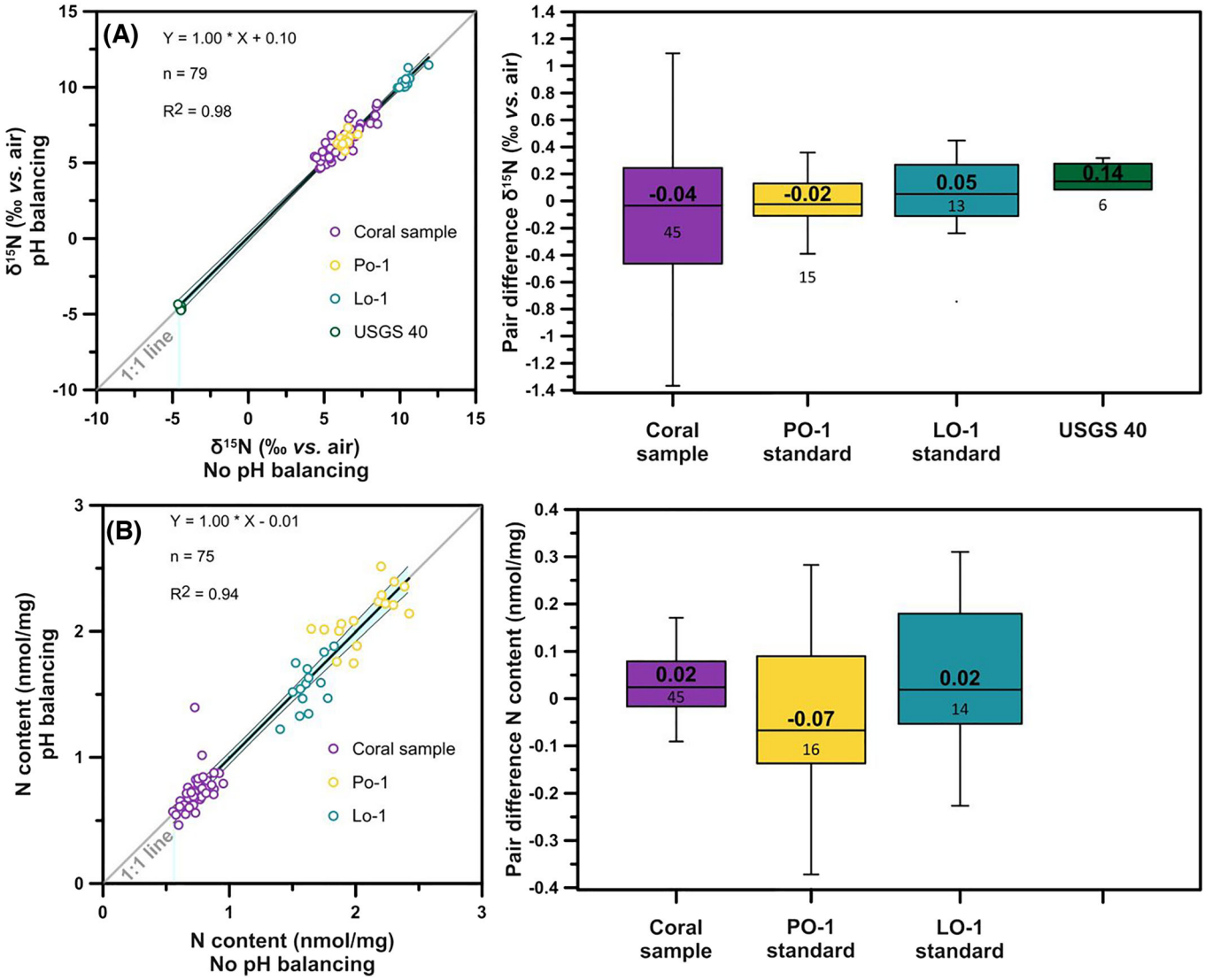

FIGURE 4 Evaluation of the effect of bypassing the pH-balancing step on $\delta^{15}N$ and weight-normalized N content. A, Left—cross-plot of $\delta^{15}N$ (‰ vs. air) results of biomineral-bound and amino acid reference material (RM). Gray line represents the theoretical 1:1 line (no difference), whereas the black line represents a least squares linear regression. Blue shading represents the 95% confidence interval of the regression. Right—box plots depicting the median difference between pH-adjusted and non-pH-adjusted sample/RM pairs, with interquartile range (IQR) and vertical bars represented as 1.5 × IQR. B, Same as panel A but for weight-normalized biomineral N content (nmol/mg). As amino acid RM USGS 40 is not biomineral-bound, N content data are not provided. [Color figure can be viewed at wileyonlinelibrary.com]

aliquots of oxidizing solution and would thus be closer to the upper limit of the envelope of optimal pH conditions of *P. chlororaphis* (Figure 3). Thus, data for all blanks presented in the next sections of this study were processed following this approach.

3.2 | Long-term stability of oxidation blanks

The updated protocol (Figure 1) produced consistent oxidation blanks (hereafter referred to as blanks) among users over 3.5 years, characterized by low N content and relatively stable $\delta^{15}N$ values. The laboratory mean of all blanks measured by eight users following the modified protocol in the period from 2019 to 2023 yielded a $\delta^{15}N$ of −2.20 ± 3.13‰ ($n = 195$) and a blank N content of 0.30 ± 0.13 nmol ($n = 195$) (Figure 5 and Table 2). A one-way ANOVA test found no statistically significant user differences for $\delta^{15}N$ when compared to the whole-laboratory mean except for user 5. N content differences among users were generally not statistically significant, with the exception of user 3 (Figures 5 and S5 [supporting information]).

We did not observe clear long-term trends in the size or $\delta^{15}N$ of the blanks. Instead, our blanks showed day-to-day variability, even for the same user. We hypothesize that the variability of blank $\delta^{15}N$ and N content could be related to variable contributions from ^{15}N-depleted atmospheric NH_3 on different days. This is supported by data presented in Figure S6 (supporting information), which shows results from in-house exposure tests (0–120 min) of oxidation vials to

TABLE 1 Comparison of pH-adjusted and non-pH-adjusted materials and their statistical significance.

	Coral sample[a]	PO-1	LO-1	USGS40
$\delta^{15}N$ (‰ vs. air)				
$\delta^{15}N$ nopH adjust (‰)	6.15 ± 1.15	6.37 ± 0.32	10.45 ± 0.50	−4.48 ± 0.036
$\delta^{15}N$ pH adjust (‰)	6.30 ± 1.12	6.39 ± 0.36	10.42 ± 0.46	−4.59 ± 0.15
n	45	15	13	6
Mean difference (‰)[b]	0.14 ± 1.60	0.02 ± 0.49	−0.03 ± 0.67	−0.11 ± 0.17
P value[c]	0.5482	0.8866	0.8749	0.1364
Weight-normalized N content (nmol/mg)				
N content no pH adjust	0.73 ± 0.09	2.08 ± 0.24	1.62 ± 0.12	...
N content pH adjust	0.72 ± 0.15	2.12 ± 0.22	1.56 ± 0.19	...
n	45	16	14	...
Mean difference (nmol/mg)[b]	−0.01 ± 0.17	0.04 ± 0.32	−0.06 ± 0.22	...
P value[c]	0.6999	0.5846	0.3428	...

[a]*Pocillopora damicornis* (Linnnaeus, 1758), non-homogenized sample matrix.
[b]Propagated error calculated as $\sigma_{1-2} = \sqrt{\sigma_1{}^2 + \sigma_2{}^2}$. Note that Figure 4 shows a box plot visualization of the median of the individual pairs, whereas here the difference is reported across whole category averages. In both cases differences are always <0.15 for both $\delta^{15}N$ (‰ vs. air) and weight-normalized N content (nmol/mg).
[c]Double-tailed unpaired *t*-test with $\alpha < 0.05$.

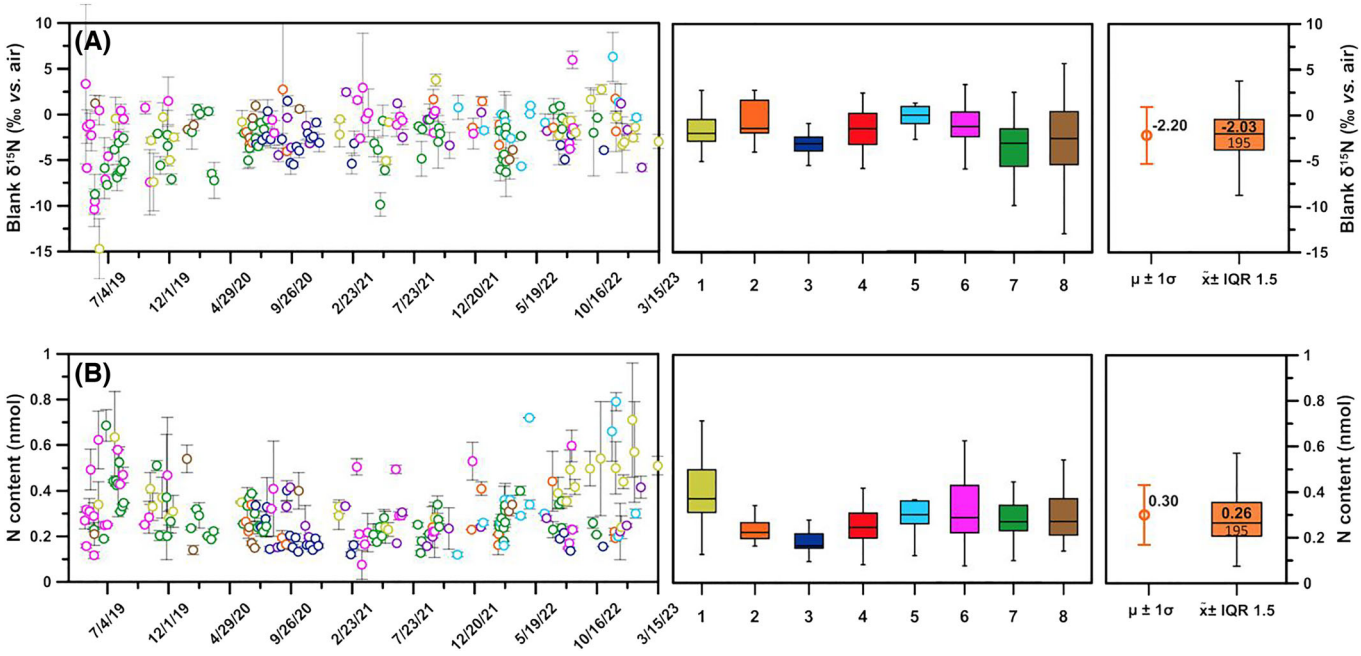

FIGURE 5 Evaluation of $\delta^{15}N$ and N content of oxidation blanks at the Max Planck Institute for Chemistry over the 2019–2023 period. A, Left—blank $\delta^{15}N$ (‰ vs. air) results over the time 2019–2023 for eight individual users using the same color code as in the central panel. Vertical bars represent 1σ envelope. Center—box plots for individual user datasets with median value, interquartile range (IQR), and vertical bars represented as 1.5 × IQR. Right—whole-laboratory $\delta^{15}N$ and N content mean (μ) and 1σ as well as conventional box plots with median ($\tilde{x}$), IQR, and vertical bars represented as 1.5 × IQR. B, Same as panel A but for oxidation blank N content (nmol). Although a small user-dependent variability is observed, for most users there are no statistically significant differences. [Color figure can be viewed at wileyonlinelibrary.com]

air inside a clean room where all oxidations are performed, which is equipped with an activated carbon and particle filter (GCS GmbH, 742 × 742 × 96 mm) to minimize exposure to airborne N species. We tested vials containing 4 M HCl, which should maximize the trapping of atmospheric NH_3, and HCl + POR, which should be more representative of the blank of a typical sample. In general, longer aerial exposure of both HCl and HCl + POR resulted in a progressive increase in N content and a decrease in blank $\delta^{15}N$ (Figure S6 [supporting information]), but the N content and $\delta^{15}N$ for a given exposure time were different on different days. These results are

TABLE 2 Observed $\delta^{15}N$ and N content values for blanks and reference materials.

ID	Material	$\delta^{15}N$ (‰ vs. air)	N content (nmol or nmol/mg)[a]
Oxidation blanks and amino acid reference materials			
Blanks	POR	−2.20 ± 3.13 ($n = 195$)	0.30 ± 0.13 ($n = 195$)
USGS 40	L-Glutamic acid	−4.69 ± 0.32 ($n = 491$)	...
USGS 65	Glycine	20.38 ± 0.36 ($n = 400$)	...
OFFSET USGS 40, 65[b]	L-Glutamic acid and glycine	−0.23 ± 0.35 ($n = 891$)	...
In-house biomineral reference materials			
PO-1	$CaCO_3$ (aragonite) POR-cleaned	6.14 ± 0.23 ($n = 180$)	2.40 ± 0.22 ($n = 180$)
PO-1	$CaCO_3$ (aragonite) NaOCl-cleaned	6.08 ± 0.21 ($n = 267$)	1.86 ± 0.20 ($n = 267$)
LO-1	$CaCO_3$ (aragonite) POR-cleaned	10.10 ± 0.29 ($n = 269$)	2.53 ± 0.24 ($n = 269$)
LO-1	$CaCO_3$ (aragonite) NaOCl-cleaned	10.20 ± 0.28 ($n = 258$)	1.43 ± 0.20 ($n = 258$)
MF-1	$CaCO_3$ (calcite) POR-cleaned	5.92 ± 0.28 ($n = 243$)	3.60 ± 0.35 ($n = 241$)
AG-Lox	$Ca_5(PO_4)_3(OH)$ (hydroxyapatite) POR-cleaned	4.06 ± 0.49 ($n = 78$)	12.49 ± 1.85 ($n = 78$)

Abbreviation: POR, persulfate oxidizing reagent.
[a]For biominerals, N content is reported as weight-normalized N content (nanomoles of N per milligram of cleaned biomineral material).
[b]Offsets reported from the respective international reference values.[6,7]

consistent with an increased contribution of atmospheric NH_3 to the blanks with increased exposure time. However, in a typical sample batch, the average user-reported exposure time during the oxidation step rarely exceeded 15 min, so the impact of atmospheric NH_3 should have been relatively low (Figure S6 [supporting information]). In addition, we do not observe a clear correlation between N content and $\delta^{15}N$ in the blanks analyzed over the past 3.5 years (Figure S7 [supporting information]). This suggests that the variability in the $\delta^{15}N$ of the blank may be related to changes in the relative contribution of different blank sources on different days. In any case, the predominantly negative $\delta^{15}N$ of the oxidation blanks is consistent with the atmosphere being the greatest source of blanks under our experimental conditions. This supports our choice of performing the oxidation in a clean room with activated charcoal filters, which we recommend for reducing the size and variability of the oxidation blanks.

In most cases the contribution of the blank to the measured $\delta^{15}N$ is minimal. For example, in a typical biomineral sample containing 10 nmol of N, the average blank of the lab (0.3 nmol and −2.20‰) would represent a fractional contribution of the blank (F_{blank}) of 3%. If the sample had a non-corrected $\delta^{15}N$ value of 5.0‰, the blank-corrected sample $\delta^{15}N$ value would be 5.2‰ (Figure S8 [supporting information]). Alternatively, if the N content of the sample was very low, or the amount of available sample material was limited, the fraction of the blank would increase, and consequently the blank correction would be larger for any given blank $\delta^{15}N$ (Figure S8 [supporting information]). A larger correction would also be needed in case the difference between the $\delta^{15}N$ values was larger, for example, in samples with very high $\delta^{15}N$. In Section 3.5, we evaluate the potential effect of a proportionally larger blank on the overall precision of the method by measuring our coral and foraminifera in-house RMs at low N quantities.

3.2.1 | Dipotassium peroxodisulfate storage and its effect on oxidation blanks

The conventional storage method for recrystallized $K_2S_2O_8$ in a desiccator reportedly resulted in a progressive increase in the N content of blanks after just a few months of storage. It has been suggested that highly hygroscopic $K_2S_2O_8$ crystals adsorb atmospheric H_2O during storage, causing partial dissolution and the formation of sulfuric acid on their surfaces,[16] thereby creating microacidic environments. Such microscopic environments would work to trap atmospheric NH_3 (as well as amines and potentially other N compounds), eventually affecting the blank. We therefore stored individual aliquots of $K_2S_2O_8$ under Ar to prevent the adsorption of H_2O and reduce atmospheric exposure. As a further precaution, we stored these aliquots in aluminum-lined vacuum bags. Long-term testing of $K_2S_2O_8$ crystals stored in this manner for ~2.5 years (Section 2.1) showed that N content of the POR blank remained very low (≤0.3 nmol) over this time span (Figure 6B). At the end of the Ar storage experiments, the N content of the blank was indistinguishable from the initial values or the whole-laboratory mean (Figure 6B), where users typically report the use of $K_2S_2O_8$ (stored under Ar atmosphere) up to a maximum of 3 months. Blank $\delta^{15}N$

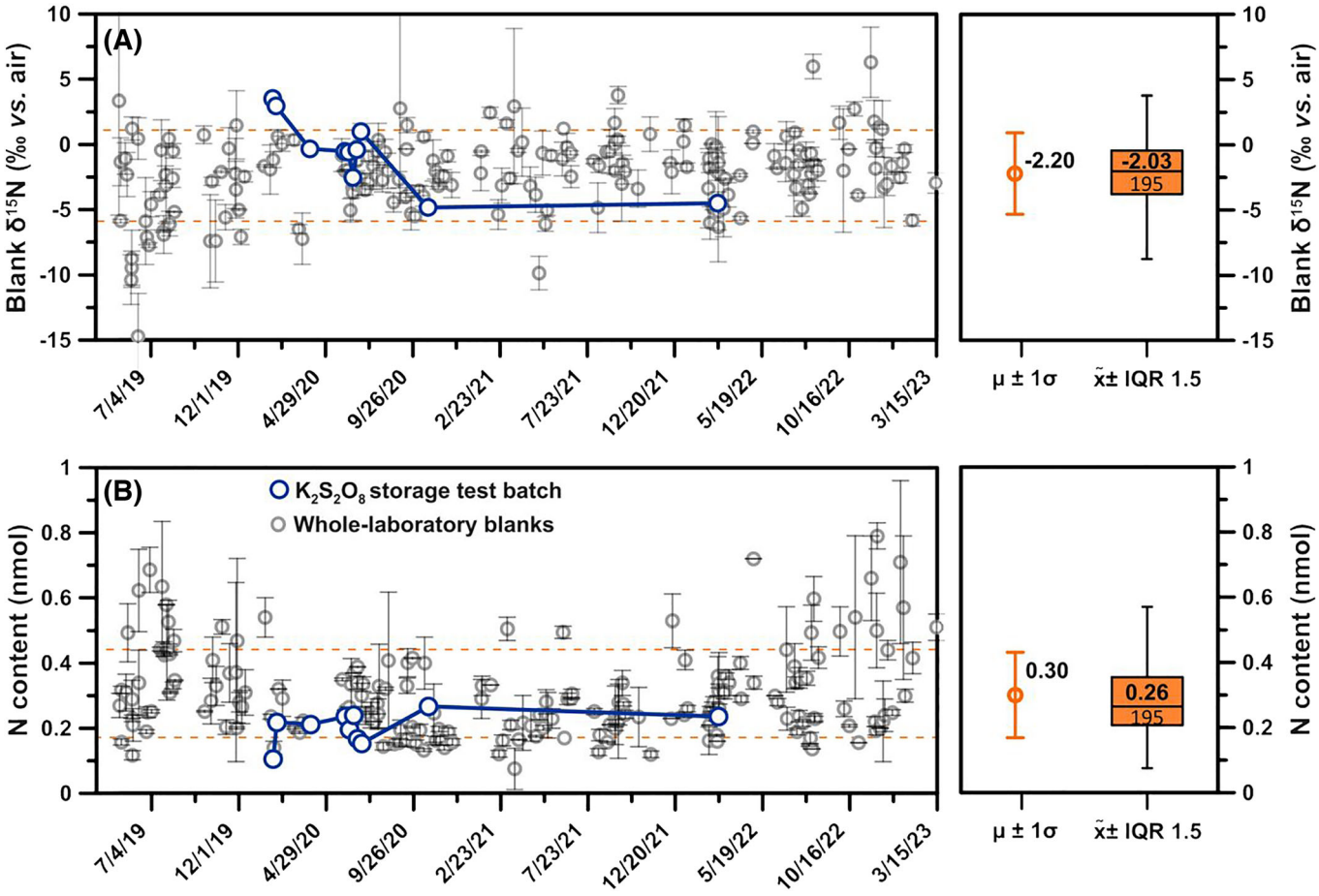

FIGURE 6 Long-term storage of dipotassium peroxodisulfate crystals in Ar atmosphere and its effect on oxidation blanks. A, Left—time series of oxidation blanks $\delta^{15}N$ for all users over the period of 2019–2023 on multiple $K_2S_2O_8$ batches as shown in Figure 5 (gray circles) and for a single batch of re-crystalized $K_2S_2O_8$ (blue circles). Orange dashed lines indicate $\pm 1\sigma$ around the mean whole-lab. Right—mean (μ) and 1 standard deviation (σ), as depicted in the right panel, which also includes conventional box plots with median ($\tilde{x}$), the interquartile range (IQR), and the error represented as 1.5 × IQR. Dashed lines represent 1σ envelope around the whole-laboratory mean. B, Same as panel A but for N content (nmol) of the oxidation blanks. [Color figure can be viewed at wileyonlinelibrary.com]

values after ~2.5 years of storage are likewise indistinguishable from the mean laboratory values (Figure 6A). The two initial $\delta^{15}N$ values at the beginning of the experiment are significantly higher than the mean of all the blanks analyzed by all users in the period 2019–2023 ($p < 0.05$ for a double-tailed unpaired t-test) (Figure 6A). However, comparing the dates in which those blanks were analyzed to the whole-laboratory time series reveals that the sample distribution lies well within the range of observed blank $\delta^{15}N$ values, and the lack of increase of N content with time further suggests that the apparent trend cannot be associated with an accumulation of contaminants on the recrystallized $K_2S_2O_8$ reagent.

3.3 | Long-term accuracy of international isotopic reference materials

Analysis of international reference amino acid RMs allows us to reconstruct the methodological accuracy of the O–D method in use at the MPIC with respect to $\delta^{15}N$. The interuser average of all RMs measured in the period from 2019 and 2023 yielded a mean $\delta^{15}N$ of −4.69 ± 0.32‰ ($n = 491$) for USGS 40 and a mean $\delta^{15}N$ of 20.38 ± 0.36‰ ($n = 400$) for USGS 65 (Figure 7 and Table 2). Over the same time period, the average offset from the reported international reference values[6,7] for both RMs combined is −0.23 ± 0.35‰.

A one-way ANOVA test for USGS 40 revealed no statistically significant differences for all users when compared to the whole-laboratory mean $\delta^{15}N$ (Figure S9 [supporting information]). For USGS 65, the same test revealed a barely significant difference for users 3 and 6. The measured offset of both USGS 40 and 65 from their respective reference values is generally indistinguishable across users with a one-way ANOVA test, with the exception of users 1 and 3 (Figure S9 [supporting information]). Overall this suggests a good consistency across users. The slightly higher standard deviation of USGS 65 (±0.36‰) with respect to USGS 40 (±0.32‰) may be ascribable to its larger $\delta^{15}N$ difference from the blank (20.68‰ vs. −2.20‰) (Figure S8 [supporting information]).

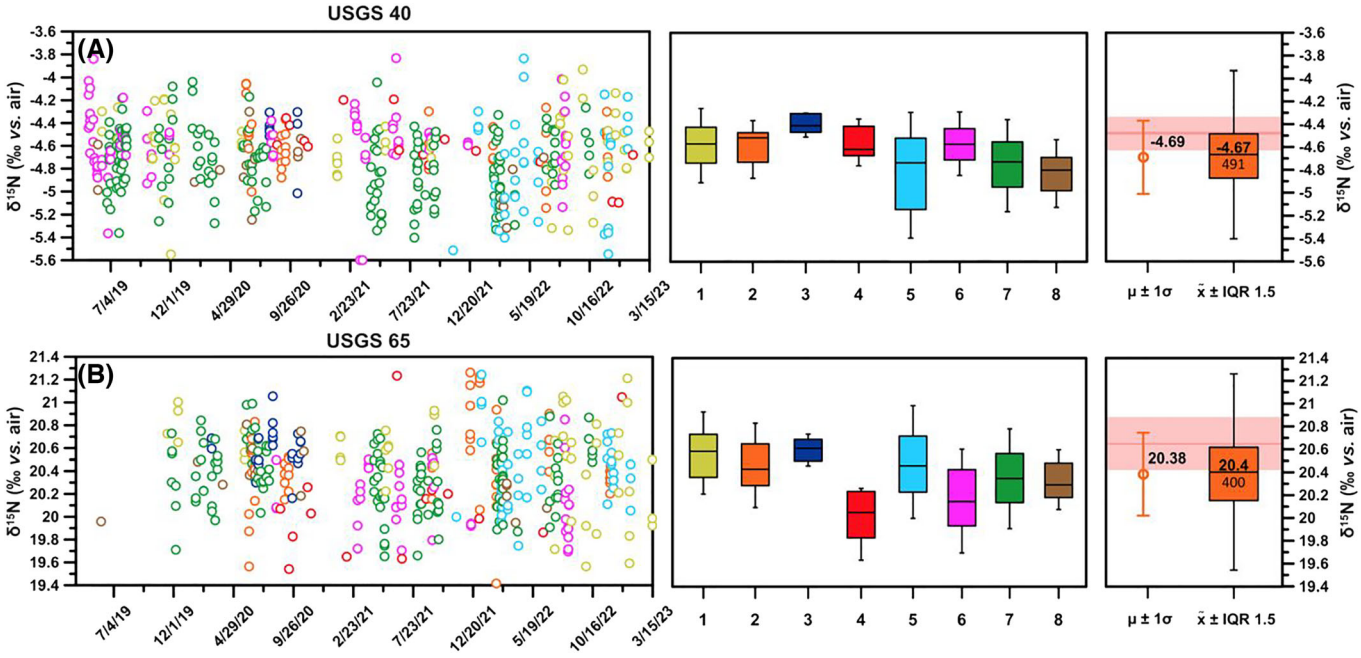

FIGURE 7 Evaluation of the long-term precision and accuracy of the oxidation–denitrifier (O–D) method at the Max Planck Institute for Chemistry over the 2019–2023 period using two international reference amino acid reference materials. A, Left—$\delta^{15}N$ (‰ vs. air) results for USGS 40 RM over ~3.5 years for eight individual lab users at the MPIC. Middle—box plots for individual users with median, interquartile range (IQR), and vertical bars represented as 1.5 × IQR. Right—whole-laboratory (all users) $\delta^{15}N$ values reported as mean (μ) and 1 standard deviation (σ) as well as conventional box plots with median ($\tilde{x}$), IQR, and vertical bars represented as 1.5 × IQR. B, Same as panel A for USGS 65. The red line and shading in the rightmost panels A and B represent the international reference values with recalculated uncertainties in 1σ. [Color figure can be viewed at wileyonlinelibrary.com]

The uncertainty reported for both USGS 40[6] and USGS 65[7] is ±0.06‰. However, in the case of USGS 40, the uncertainty was reported as the average of standard deviations across five measurement sessions from two laboratories. For USGS 65, the uncertainty is based on Bayesian random effect statistical analysis on data contributed by nine different laboratories. For comparability with our $\delta^{15}N$ measurements, we recalculated the standard deviation of the interlaboratory mean of these RMs with the same error propagation starting from the mean results of the individual laboratories. We obtain an RM uncertainty of ±0.15‰ for USGS 40 and ±0.36‰ USGS 65, which are displayed in Figure 8.

It is worth noting that international reference $\delta^{15}N$ values of the amino acid RMs used here have been analyzed with conventional EA techniques[6,7] and thus required ~100 μmol of N for measurement. The values reported here for the same RMs using the O–D method are based on the sample size in the 1–20 nmol range (Section 3.5), which are three orders of magnitude smaller (Figure 8). Thus, our results indicate that our method produced data with temporally consistent accuracy and precision. Because our average values and the reference values are within 1σ analytical precision of each other (Figure 8), we do not apply any correction for this small offset.

3.4 | Long-term consistency of biomineral-bound $\delta^{15}N$ and N content in biomineral in-house reference materials

The analysis of organic N bound in the crystalline structure of biominerals requires that any given sample be chemically precleaned to remove nonbound exogenous organic matter, given the potential for large differences in $\delta^{15}N$ between these two pools of organic N.[62,63] However, the choice of appropriate chemical cleaning is dependent on the type of biomineral analyzed, the types of contamination expected, and the diagenetic conditions the biomineral and its sediment matrix have experienced. For example, opaline diatoms dissolve under basic conditions and thus require that cleaning occur under acidic conditions. Consistent with this expectation, cleaning with perchloric acid of diatom opal gives more reproducible, stable results than cleaning with Na-hypochlorite (NaOCl), which generates a basic solution.[63] For foraminifera, which are composed of calcite, Ren et al.[26] showed that a reductive cleaning, followed by either NaOCl or POR oxidative cleaning, produced equivalent results for both BB-$\delta^{15}N$ and weight-normalized biomineral N content (nanomoles of N per milligram of cleaned biomineral material). Since then, POR cleaning has been the predominant choice for foraminifera-bound $\delta^{15}N$.[17,23,24,27] For corals, similar testing showed negligible

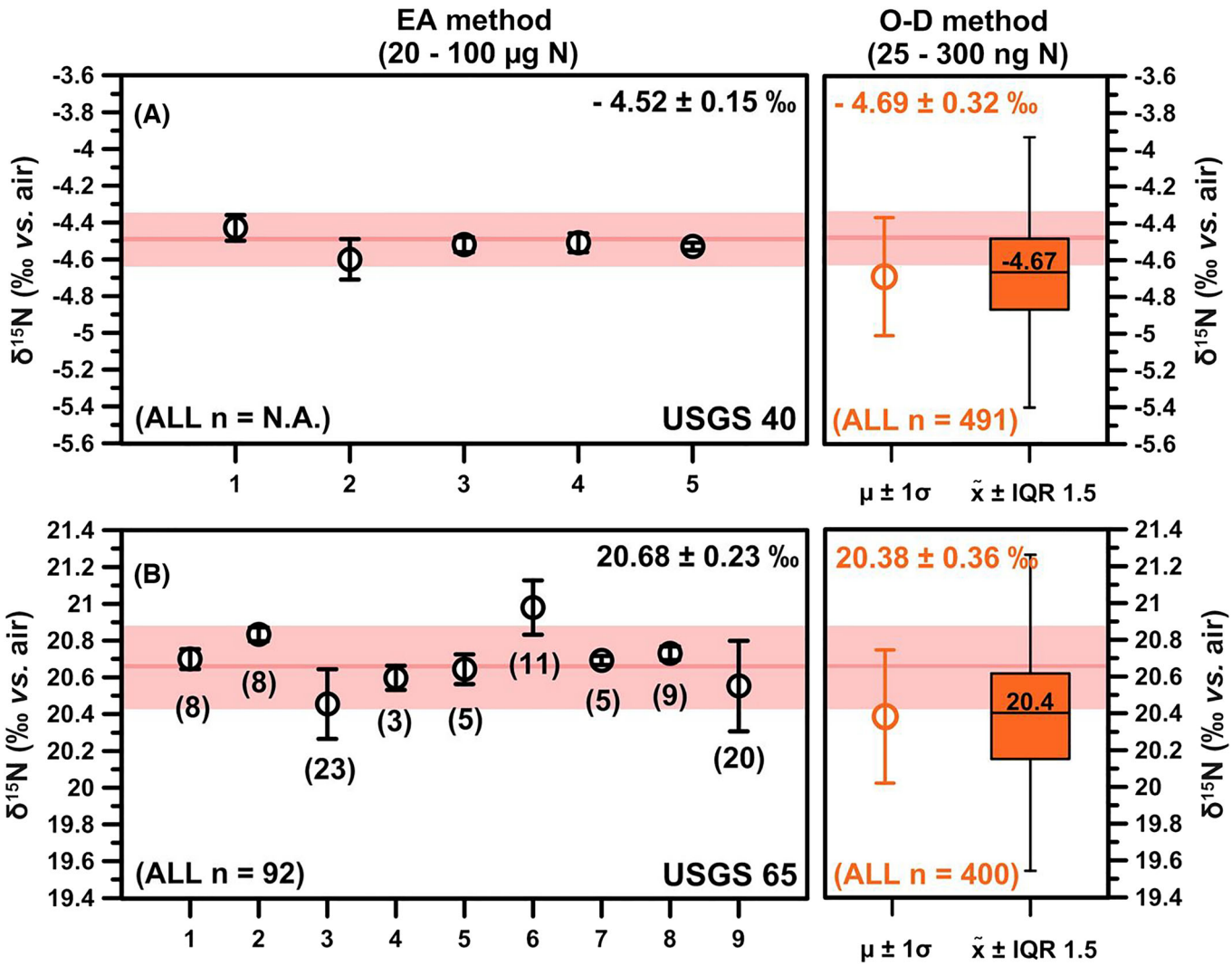

FIGURE 8 Published interlaboratory analyses of $\delta^{15}N$ in amino acid reference materials USGS 40 and 65. A, Left—1 to 3 represent three measurement sessions in one laboratory and 4 to 5 for different laboratories for USGS 40. Vertical bars represent 1σ uncertainty. Right—box plot for the Max Planck Institute for Chemistry whole-laboratory $\delta^{15}N$ values reported in mean (μ) and 1 standard deviation (σ) as well as conventional box plots with median ($\tilde{x}$), interquartile range (IQR), and vertical bars represented as 1.5 × IQR in orange. The red line represents the reported reference value in Qi et al.[6] As individual measurements were not available, recalculated uncertainty with error propagation $\sigma_\mu = \sqrt{\sigma_1{}^2 + \sigma_2{}^2 + \cdots + \sigma_5{}^2}$ of the individual means is applied. B, Left—nine independent laboratories contributed to $\delta^{15}N$ analysis of USGS 65 with elemental-analyzer techniques for a total of 92 measurements.[7] Vertical bars represent 1σ uncertainty, and values between brackets are the reported number of measurements for each lab. The total uncertainty (1σ) is recalculated on the mean of the whole dataset ($n = 92$). Right—same as in A but for USGS 65. [Color figure can be viewed at wileyonlinelibrary.com]

differences across NaOCl and POR oxidative cleaning for both BB-$\delta^{15}N$ and weight-normalized N content,[41] and NaOCl has been established as the commonly used method for both deep-sea scleractinian corals[64] and shallow-water scleractinia,[41] with an additional reductive cleaning step for the former but not for the latter. For tooth enamel hydroxyapatite/fluorapatite, a reductive cleaning coupled with a POR oxidative cleaning has commonly been used.[45,47] A summary of chemical cleaning methods and equipment utilized in this work can be found in Tables S1 and S2 (supporting information).

We have used in-house carbonate and enamel biomineral RMs to evaluate the analytical reproducibility of the O–D method (cleaning, oxidation, injection to bacteria, and measurement using IRMS). The impact of chemical cleaning on long-term reproducibility is thus implicitly constrained by this measurement; next, we detail the results of the analysis of two coral aragonitic materials (PO-1 and LO-1), one calcitic foraminifera RM (MF-1), and one hydroxyapatite RM (AG-Lox) over a ~3.5-year period by eight individual users, which are shown in Figure 9 and summarized in Table 2.

The analysis of the two coral RMs in the period from 2019 and 2023 yielded a mean interuser BB-$\delta^{15}N$ of 6.08 ± 0.21‰ ($n = 267$) and 10.20 ± 0.28‰ ($n = 258$) for NaOCl-cleaned PO-1 and LO-1, respectively (Figure 9 and Table 2). The uncertainties reported here for our modified method are compatible with reported values of the previous method at Princeton University (~0.2‰) for another in-

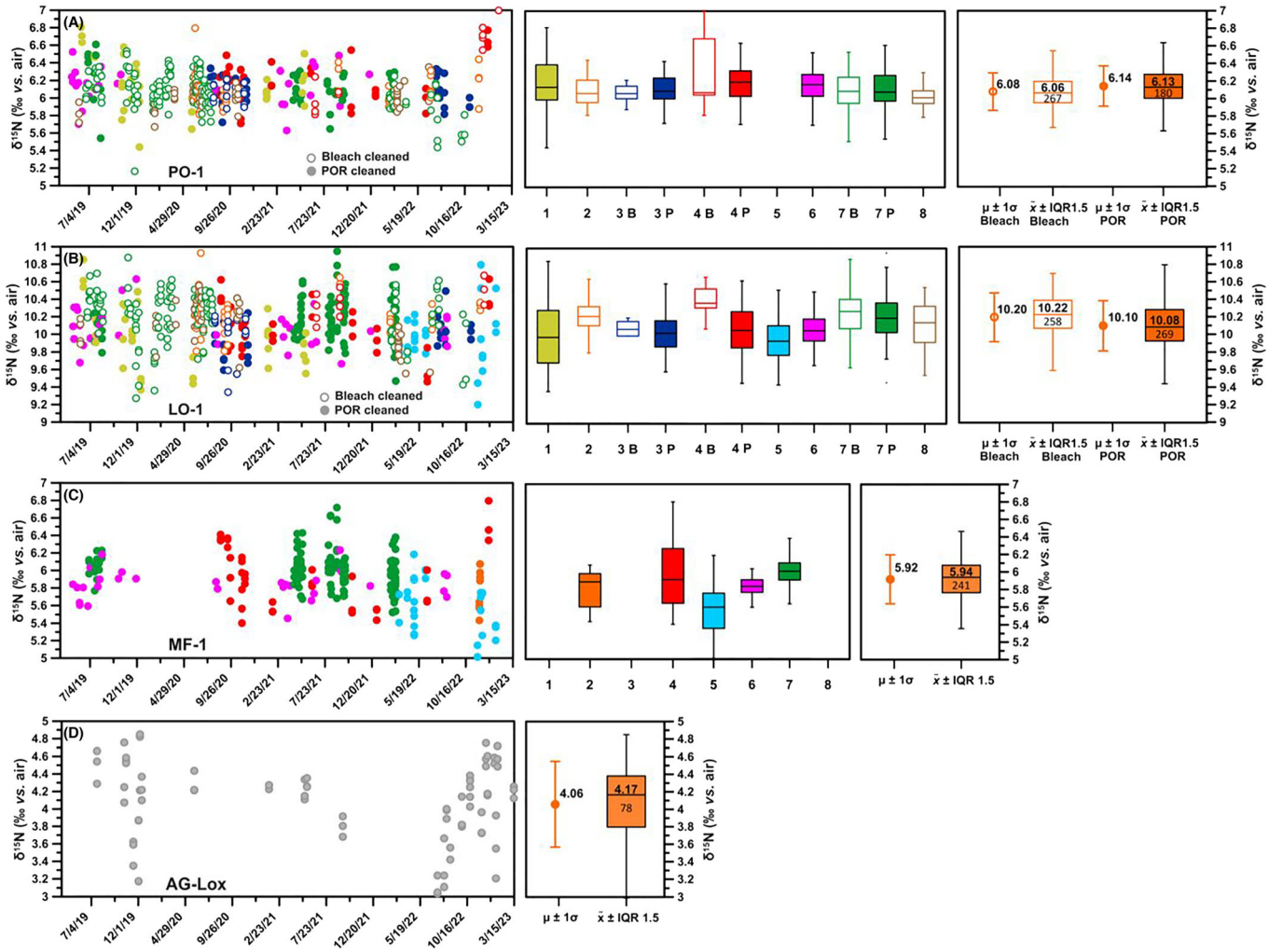

FIGURE 9 Evaluation of the long-term analytical precision of BB-$\delta^{15}N$ measurements of four biomineral in-house reference materials (RM) using the oxidation–denitrifier method at the Max Planck Institute for Chemistry over the 2019–2023 period. A, Left—BB-$\delta^{15}N$ (‰ vs. air) results from NaOCl (open symbols) and persulfate oxidizing reagent (POR)–cleaned (filled symbols) PO-1 coral RM over ~3.5 years for eight individual lab users at the MPIC. Middle—box plots for individual user datasets with median, interquartile range (IQR), and vertical bars represented as 1.5 × IQR for POR cleaning (filled box, P) and NaOCl cleaning (empty box, B). Right—whole-laboratory (all users) $\delta^{15}N$ values reported in mean (μ) and 1 standard deviation (σ) as well as conventional box plots with median ($\tilde{x}$), IQR, and vertical bars represented as 1.5 × IQR. B, Same as panel A but for NaOCl- and POR-cleaned LO-1 coral RM. C, Same as panel A but for POR-cleaned MF-1 foraminifera RM. D, Same as panel A but for POR-cleaned AG-Lox tooth hydroxyapatite RM. The middle panel is not shown here as all measurements were performed by a single user (#1). [Color figure can be viewed at wileyonlinelibrary.com]

house coral RM (CBS-1), also cleaned with NaOCl.[31] PO-1 and LO-1 RMs were also repeatedly cleaned with POR during the same period to compare the two cleaning methods. The interuser average of PO-1 and LO-1 coral RMs cleaned in this manner yielded a mean BB-$\delta^{15}N$ of 6.14 ± 0.23‰ (n = 180) and 10.10 ± 0.29‰ (n = 269) for POR-cleaned PO-1 and LO-1, respectively. Long-term monitoring of CBS-1 coral RM with POR cleaning at Princeton University[45] gave a similar reproducibility (±0.3‰) to what we observed with this method. Although the BB-$\delta^{15}N$ differences (POR − NaOCl) are extremely small (0.06 ± 0.31‰ for PO-1 and −0.09 ± 0.40‰ for LO-1), the BB-$\delta^{15}N$ of NaOCl-cleaned and POR-cleaned samples are statistically different ($p < 0.05$) from each other due to the high number of measurements (Table S4 [supporting information]). These differences are much smaller than the analytical precision of the O–D method and can be considered negligible for practical applications.

Significant differences were observed for the weight-normalized N content of these materials across treatments. NaOCl-cleaned PO-1 and LO-1 RMs were consistently lower in weight-normalized N content than those cleaned with POR (Figure 10 and Table 2). The whole-laboratory average of PO-1 in the period from 2019 and 2023 yielded a mean weight-normalized N content of 2.40 ± 0.22nmol (n = 180) for POR cleaning and 1.86 ± 0.20 nmol (n = 267) for NaOCl cleaning. The same analysis for LO-1 yielded a mean weight-normalized N content of 2.53 ± 0.24 nmol (n = 269) for POR cleaning and 1.43 ± 0.20 nmol (n = 258) for NaOCl cleaning (Figure 9 and Table 2). The cause of such an important N content difference

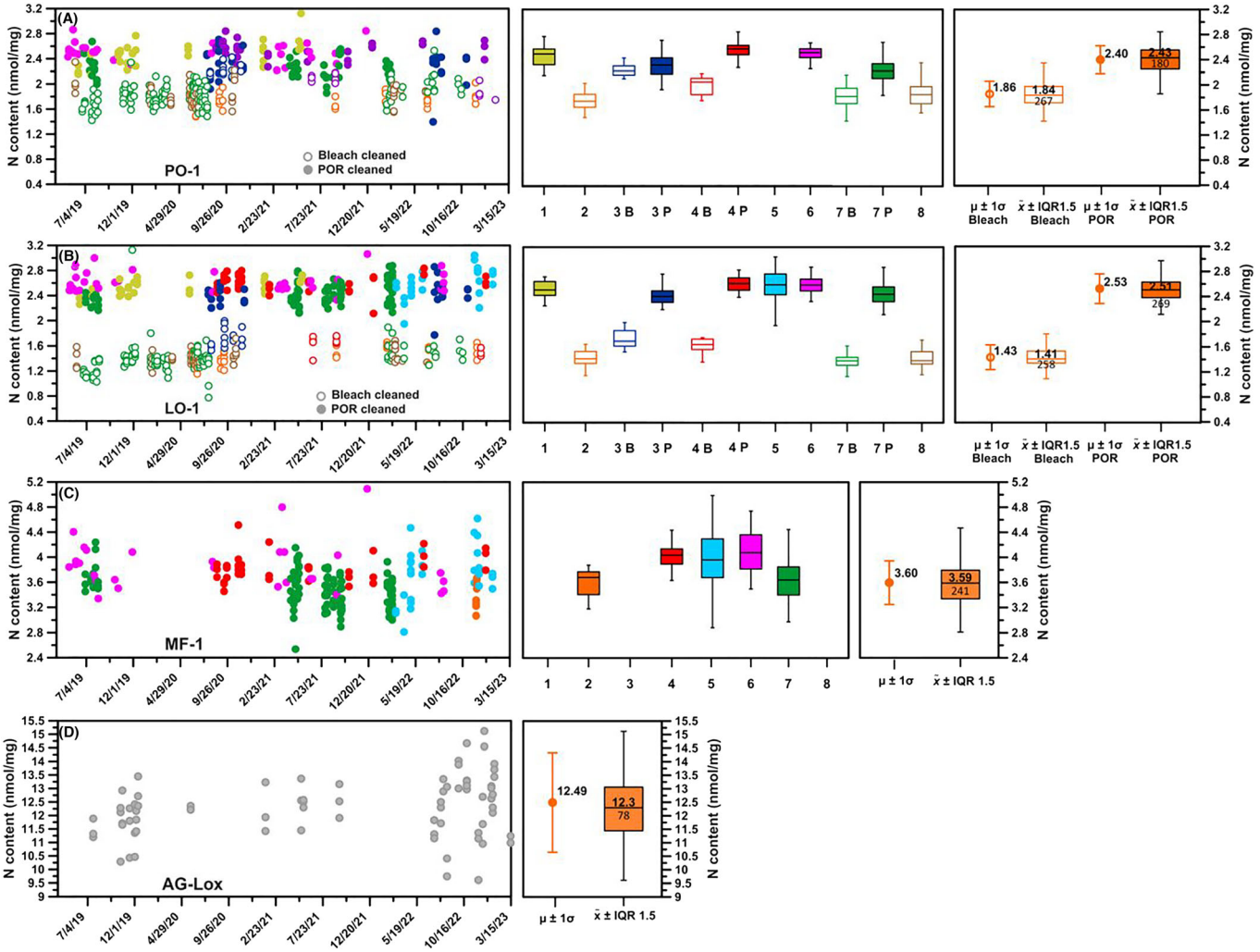

FIGURE 10 Evaluation of the long-term analytical precision of weight-normalized N content measurements of four biomineral in-house reference materials (RM) using the oxidation–denitrifier method at the Max Planck Institute for Chemistry over the 2019–2023 period. A, Left—weight-normalized N content (nmol/mg) results from NaOCl (open symbols) and persulfate oxidizing reagent (POR)–cleaned (filled symbols) PO-1 coral RM over ~3.5 years for eight individual lab users at the MPIC. Middle—box plots for individual user datasets with median, interquartile range (IQR), and vertical bars represented as 1.5 × IQR for POR cleaning (filled box, P) and NaOCl cleaning (empty box, B). Right—whole-laboratory (all users) weight-normalized N content values reported in mean (μ) and 1 standard deviation (σ) as well as conventional box plots with median ($\tilde{x}$), IQR, and vertical bars represented as 1.5 × IQR. B, Same as panel A but for NaOCl- and POR-cleaned LO-1 coral RM. C, Same as panel A but for POR-cleaned MF-1 foraminifera RM. D, Same as panel A but for POR-cleaned AG-Lox tooth hydroxyapatite RM. The middle panel is not shown here as all measurements were performed by a single user (#1). [Color figure can be viewed at wileyonlinelibrary.com]

remains unclear, particularly when considered alongside an effectively negligible $\delta^{15}N$ difference across treatments for the same coral RMs. One possibility has to do with the mineral structure of PO-1 and LO-1. The skeleton of scleractinian corals is mostly composed of aragonite.[65] Despite being stable in ambient conditions, high temperatures (120°C) over the 65 min autoclave cycle used for POR oxidative cleaning might either induce partial dissolution and recrystallization of the aragonitic mineral matrix of coral RMs[66] and/or partial dissolution of the borosilicate vial in the high pH of the POR solution. It is possible that the formation of secondary mineral or noncrystalline phases during this process might result in the trapping of organic matter, thereby allowing for a greater weight-normalized N content than the same RMs cleaned at room temperature with NaOCl treatment. For example, it has been suspected that in aragonitic otoliths from certain fish species, POR- and autoclave-based cleaning causes recrystallization to calcite, resulting in N trapping, an effect not seen with NaOCl cleaning.[51]

To investigate these questions, we performed Fourier-transform infrared (FTIR) spectroscopy and scanning electron microscopy (SEM) analyses of pristine (uncleaned) and POR-cleaned PO-1 and LO-1 coral RMs. A clear change in the IR spectrum of coral aragonite occurred upon POR cleaning, but no difference from the pristine RM is observed after NaOCl treatment (Figure S10 [supporting information]). The added FTIR features in POR-cleaned RMs are identified as calcium silicate hydrate (CSH) phases.[67] This suggests that partial dissolution of the borosilicate vials during POR cleaning is

at least partially responsible for the higher N contents, which is consistent with experimental precipitation of CSH from aqueous solutions in similar high-pH environments rich in Ca and silica (SiO_2).[68] CSH precipitates appear to occur homogeneously onto crystal surfaces based on SEM imaging (Figure S14 [supporting information]). No recrystallization of aragonite to calcite is observed in PO-1 and LO-1 (Figure S10 [supporting information]). In contrast, the fact that the $\delta^{15}N$ offset between NaOCl- and POR-cleaning methods was less than 0.1‰ argues that the N trapped (or added) during POR cleaning is native to the coral, implying that this process likely occurs when most of the exogenous organic matter has already been removed (Table S4 [supporting information]).

Unlike the PO-1 and LO-1 RMs, MF-1 was cleaned only with POR during the experimental period 2019–2023, making this treatment the most established cleaning method for foraminifera.[26] The laboratory means of BB-$\delta^{15}N$ and weight-normalized N content for this POR-cleaned RM at the end of the 3.5-year observation period were 5.92 ± 0.28‰ ($n = 243$) and 3.60 ± 0.35 nmol ($n = 241$), respectively. Before the MF-1 RM became available, reproducibility was assessed as the average standard deviation

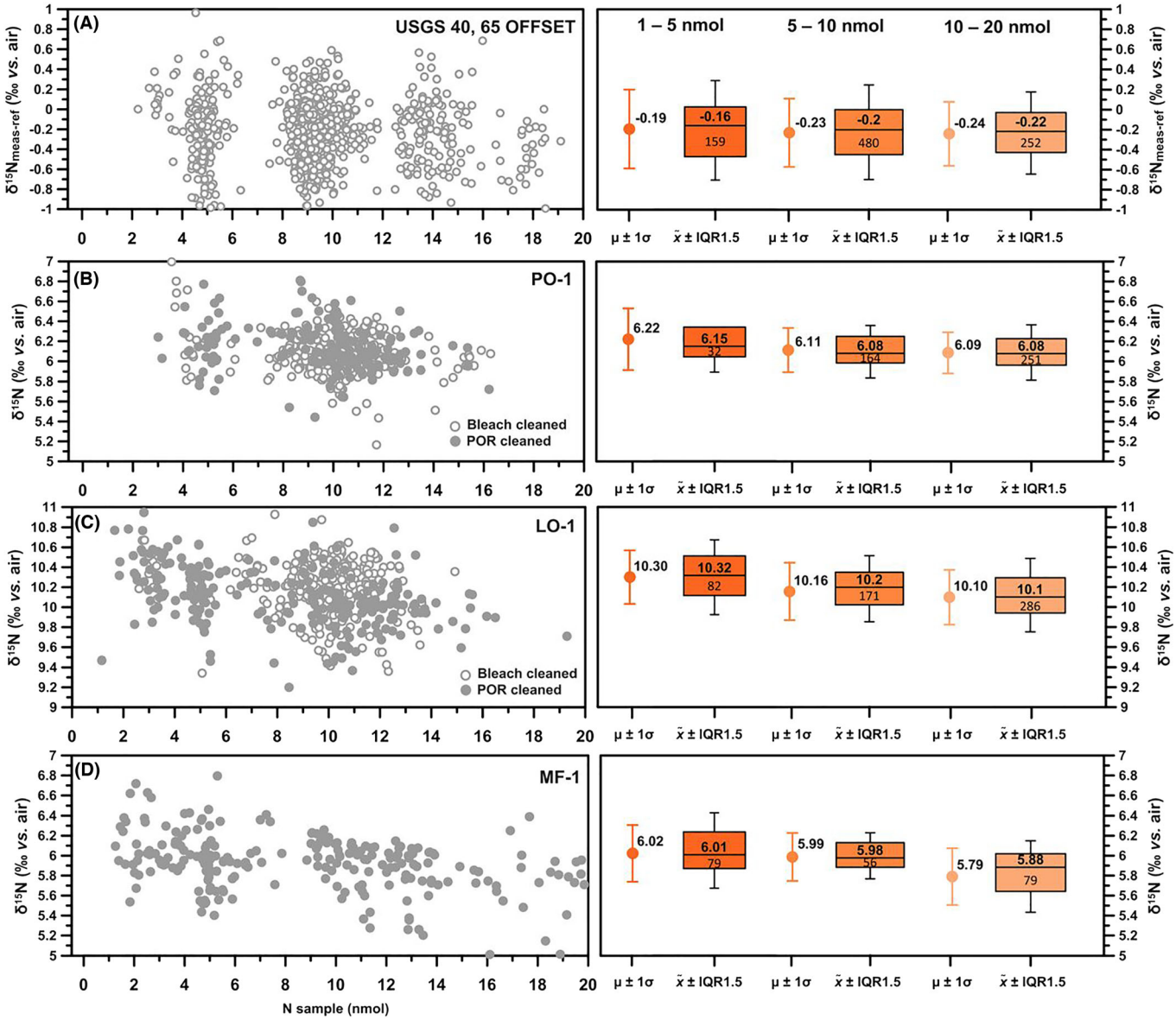

FIGURE 11 Evaluation of analytical precision of $\delta^{15}N$ measurements at different concentrations (1–20 nmol) using international reference amino acid and biomineral in-house reference materials (RM). A, Left—combined USGS 40 and 65 offsets from their relative international reference values as a function of sample size (nmol). Right—box plots depicting the median $\delta^{15}N$ (‰ vs. air) values for three distinct sample size categories (1–5, 5–10, and 10–20 nmol), reported in mean (μ) and 1 standard deviation (σ) as well as conventional box plots with median ($\tilde{x}$), interquartile range (IQR), and vertical bars represented as 1.5 × IQR. B, C, Same as in A but for PO-1 and LO-1 coral RMs. The box plot refers to the combined NaOCl and persulfate oxidizing reagent–cleaned datasets. D, Same as in B and C but for foraminifera MF-1 RM. No cleaning is applies to RMs in panel A. [Color figure can be viewed at wileyonlinelibrary.com]

estimated from the means of duplicate measurements. The average standard deviation of replicated foraminifera-bound $\delta^{15}N$ measurements reported by Ren et al[26] (±0.3‰), Martínez-García et al[24] (±0.19‰), Ren et al[25] (±0.22‰), and Farmer et al[20] (±0.22‰) is similar to the long-term interuser reproducibility of our foraminifera RM reported here (±0.28‰; Figure 9C). It is worth noting that contrary to our reported estimations, most previously published uncertainties were based on replicates of the same samples after cleaning, thereby not representative of the full procedural blank. In light of an increasing number of recent foraminifera studies published with BB-$\delta^{15}N$ over the past decade,[17,23,24,29,30,69] we propose MF-1 foraminifera RM as an RM to monitor both intra- and interlaboratory reproducibility for future foraminifera-based $\delta^{15}N$ studies. Data for POR-cleaned MF-1 are available only for the 2019–2023 period, so we undertook a dedicated comparative test of NaOCl and POR treatments for this RM. FTIR analysis on MF-1 revealed the same pattern observed in PO-1 and LO-1 between NaOCl and POR cleaning, with the presence of CSH in the latter but not in the former (Figure S11 [supporting information]). Testing also revealed a higher N content for MF-1 for POR cleaning (Figure S13 [supporting information]).

The AG-Lox tooth enamel RM was also cleaned only with POR over the period of 2019–2023. The laboratory mean for this RM was 4.06 ± 0.49‰ ($n = 78$) for $\delta^{15}N$ and 12.49 ± 1.85 nmol ($n = 78$) for weight-normalized N content (Figures 10D and 11D). Given the novelty of the application,[47] there are no enamel-bound N comparisons available in the literature, but a shark tooth enameloid in-house RM cleaned with POR at Princeton University[45] using the previous methodology yielded a comparable but slightly poorer reproducibility (±0.7‰). A dedicated test for the impact of NaOCl and POR cleaning on Ag-Lox revealed small amounts of CSH in this material as well (Figure S12 [supporting information]), as confirmed by SEM imaging (Figure S14 [supporting information]).

Long-term monitoring (Figure 10) and specific testing on all RMs (Figure S13 [supporting information]) revealed that N content is consistently higher in POR-cleaned samples than in NaOCl-cleaned samples. However, across all biominerals analyzed in this study, BB-$\delta^{15}N$ is not affected by the choice of cleaning. Given that higher N content appears to be associated with the presence of contaminant CSH in POR-cleaned material (Figure S14 [supporting information]), NaOCl could represent a more suitable cleaning method for aragonitic, calcitic, and hydroxyapatite biominerals. However, our testing might not account for all possible variations in sample matrix effects, given that all the RMs analyzed in this study correspond to relatively young fossils. We advise for the testing of both cleaning methods on splits of the same samples before the initiation of a specific project.

Overall, the results of the analysis of biomineral in-house RMs indicate that our modified method ("sandwich," pH-balance bypass, and $K_2S_2O_8$ storage) can be used to increase sample throughput without compromising analytical precision.

3.5 | Method performance at low N concentrations

As noted earlier, the value of widely used RMs such as USGS 40 and USGS 65 are reported by users employing an EA-coupled IRMS, which typically requires micromole concentrations of N.[6,7] The O–D method allows for the analysis of 1–2 nmol amounts of analyte N, three orders of magnitude lower than conventional EA techniques. However, as the sample size decreases, the relative contribution of

TABLE 3 Comparison of $\delta^{15}N$ differences across sample size categories of measured reference materials.

	n1, n2, n3[a]	1–5 nmol (‰)	5–10 nmol (‰)	10–20 nmol (‰)
	Mean value			
PO-1	32, 164, 251	6.22 ± 0.31	6.11 ± 0.22	6.09 ± 0.21
LO-1	79, 168, 280	10.30 ± 0.27	10.16 ± 0.29	10.10 ± 0.27
MF-1	78, 55, 78	6.02 ± 0.28	5.99 ± 0.24	5.79 ± 0.28
USGS 40 + 65 offsets	159, 480, 252	−0.19 ± 0.40	−0.23 ± 0.34	−0.24 ± 0.32
	n1, n2, n3[a]	1–5 versus 5–10 nmol (‰)	1–5 versus 10–20 nmol (‰)	5–10 versus 10–20 nmol (‰)
	Mean difference size classes[b]			
PO-1	32, 164, 251	0.11 ± 0.38	0.14 ± 0.37	0.03 ± 0.30
LO-1	79, 168, 280	0.14 ± 0.39	0.20 ± 0.38	0.06 ± 0.40
MF-1	78, 55, 78	0.04 ± 0.37	0.23 ± 0.40	0.20 ± 0.37
USGS 40 + 65 offsets	159, 480, 252	0.04 ± 0.52	0.05 ± 0.51	0.01 ± 0.47

[a]n1 for 1–5 nmol, n2 for 5–10 nmol, and n3 for 10–20 nmol.
[b]Propagated error calculated as $\sigma_{1-2} = \sqrt{{\sigma_1}^2 + {\sigma_2}^2}$; values in ‰ versus air.

the procedural blank increases, and the blank correction becomes larger (Figure S8 [supporting information]). Although measurements in the IRMS are typically performed using around 5 nmol of N, we typically target around 10–15 nmol of N in each sample to minimize the effect of the blank correction (Figure S8 [supporting information]). In this section, we evaluate the performance of the O–D method over the range of 1 to 20 nmol of N.

We divide our dataset into three categories: 1–5, 5–10, and 10–20 nmol N. For the amino acid RMs USGS 40 and USGS 65, the values obtained were statistically indistinguishable between all three categories, demonstrating that our blank correction is robust, even in cases where the contribution of the blank is as high as 10% (Figure 11 and Table 3). For BB-δ^{15}N measurements of our in-house biomineral RMs, the difference between the mean of these categories was always ≤0.2‰ for all RMs, which lies within the reported 1σ analytical precision of our measurements. This suggests that our blank correction provides a good approximation of the analytical blank for the entire procedure. Although the differences between the different categories are within our analytical uncertainty, in some cases, they are statistically significant. Because no significant differences were observed in the case of the amino acid RMs, this observation suggests that the cleaning step may be introducing a small additional blank. In any case, its potential impact on the estimated BB-δ^{15}N would be minimal even in the case of small samples (i.e., increasing from 0.14 ± 0.37‰ to 0.23 ± 0.40‰). It is also worth noting that our dataset shows no change in the precision of the measurements across the three different sample size categories analyzed (Figure 11 and Table 3).

4 | CONCLUDING REMARKS

The analytical changes outlined improve the existing methodology for the analysis of BB-δ^{15}N. These include (a) a consistent way of sealing the oxidation environment for the conversion of organic N to NO_3^-, (b) bypassing of the pH adjusting of the NO_3^- solutions to be amended to denitrifying bacteria, and (c) improved storage of $K_2S_2O_8$ crystals used for the preparation of the POR reagent. Collectively, these changes result in a methodology that increases sample throughput without compromising analytical precision. We also report the development of and in-house results from multiple biomineral RMs, which provide a framework for long-term monitoring, future methodological work, and intercalibration.

ACKNOWLEDGMENTS

We are grateful to Taihun Kim for providing the *Porites* sp. coral material used to generate the PO-1 RM and to Anne Lorrain and Valentine Meunier for providing *Pocillopora damicornis* coral samples used for pH-balancing experiments (samples collected during the research cruise: IGUANE aboard R/V ALIS, DOI: 10.17600/18000897). We are grateful to Hubert Vonhof for providing *Lophelia pertusa* coral samples for generating standard LO-1. We are grateful to Thomas Tütken for providing material for the AG-Lox RM and to Björn Taphorn for the help in the preparation of the MF-1 RM. We thank Thomas Leutert, Michelle Meffert, Alina Jaeger, Denise Radermacher, Noémie Joseph Dit Choisnard and Sitara Schmidt for their help in the laboratory in the early stage of this work and to Anna Golub and Noreen Garcia for their help in the latest stages. We thank Crystal Rao and Mason Scher for helpful discussions and Haojia (Abby) Ren, Xingchen (Tony) Wang, Emma R. Kast, and Alexandra Weigand for their continued contributions to methodological improvements. We thank Vasily Minkov and Mikhail Eremets for the use of their SEM and help with image acquisition. We are grateful to Anja Studer and an anonymous reviewer for their detailed and constructive reviews of this manuscript. This work was funded by the Max Planck Society (A.M.G.). The authors also acknowledge funding from the Deutsche Forschungsgemeinschaft (DFG) Project number 468591845 (A.M.G.)- - SPP2299/44183248, the Emmy Noether Fellowship LU 2199/2-1 (T.L) and the Paul Crutzen Nobel Prize Postdoctoral Fellowship (N.D.). Open Access funding enabled and organized by Projekt DEAL.

PEER REVIEW

The peer review history for this article is available at https://www.webofscience.com/api/gateway/wos/peer-review/10.1002/rcm.9650.

DATA AVAILABILITY STATEMENT

The data that support the findings of this study are openly available in EDMOND at https://doi.org/10.17617/3.OMF3JWM.

ORCID

Simone Moretti https://orcid.org/0000-0002-6772-7269
Nicolas N. Duprey https://orcid.org/0000-0002-1109-0772
Alan D. Foreman https://orcid.org/0000-0002-5082-5786
Anthea Arns https://orcid.org/0000-0002-8172-6027
Jonathan Jung https://orcid.org/0000-0002-2739-9926
Xuyuan E. Ai https://orcid.org/0000-0003-1353-6114
Alexandra Auderset https://orcid.org/0000-0002-6316-4980
Jesse Farmer https://orcid.org/0000-0001-5200-6429
Jennifer Leichliter https://orcid.org/0000-0001-9373-8634
Tina Lüdecke https://orcid.org/0000-0002-9165-2586
Tanja Wald https://orcid.org/0000-0002-1774-4749
Maayan Yehudai https://orcid.org/0000-0003-3252-3458
Daniel M. Sigman https://orcid.org/0000-0002-7923-1973
Alfredo Martínez-García https://orcid.org/0000-0002-7206-5079

REFERENCES

1. Ambrose SH. Stable carbon and nitrogen isotope analysis of human and animal diet in Africa. *J Hum Evol*. 1986;15(8):707-731. doi:10.1016/S0047-2484(86)80006-9
2. Casciotti KL. Nitrogen and oxygen isotopic studies of the marine nitrogen cycle. *Ann Rev Mar Sci*. 2016;8(1):379-407. doi:10.1146/annurev-marine-010213-135052
3. Deniro MJ, Epstein S. Influence of diet on the distribution of nitrogen isotopes in animals. *Geochim Cosmochim Acta*. 1981;45(3):341-351. doi:10.1016/0016-7037(81)90244-1

4. Ferrier-Pagès C, Leal MC. Stable isotopes as tracers of trophic interactions in marine mutualistic symbioses. *Ecol Evol*. 2019;9(1):723-740. doi:10.1002/ece3.4712
5. Sigman DM, Fripiat F. Nitrogen isotopes in the ocean. In: Cochran JK, Bokuniewicz HJ, Yager PL, eds. *Encyclopedia of Ocean Sciences*. Third ed. Academic Press; 2019:263-278. doi:10.1016/B978-0-12-409548-9.11605-7
6. Qi H, Coplen TB, Geilmann H, Brand WA, Böhlke JK. Two new organic reference materials for δ13C and δ15N measurements and a new value for the δ13C of NBS 22 oil. *Rapid Commun Mass Spectrom*. 2003;17(22):2483-2487. doi:10.1002/rcm.1219
7. Schimmelmann A, Qi H, Coplen TB, et al. Organic reference materials for hydrogen, carbon, and nitrogen stable isotope-ratio measurements: caffeines, n-alkanes, fatty acid methyl esters, glycines, l-valines, polyethylenes, and oils. *Anal Chem*. 2016;88(8):4294-4302. doi:10.1021/acs.analchem.5b04392
8. Casciotti KL, Sigman DM, Hastings MG, Böhlke JK, Hilkert A. Measurement of the oxygen isotopic composition of nitrate in seawater and freshwater using the denitrifier method. *Anal Chem*. 2002;74(19):4905-4912. doi:10.1021/ac020113w
9. Sigman DM, Casciotti KL, Andreani M, Barford C, Galanter M, Böhlke JK. A bacterial method for the nitrogen isotopic analysis of nitrate in seawater and freshwater. *Anal Chem*. 2001;73(17):4145-4153. doi:10.1021/ac010088e
10. Christensen S, Tiedje JM. Sub-parts-per-billion nitrate method: use of an N_2O-producing denitrifier to convert NO_3^- or $^{15}NO_3^-$ to N_2O. *Appl Environ Microbiol*. 1988;54(6). doi:10.1128/aem.54.6.1409-1413.1988
11. McIlvin MR, Casciotti KL. Technical updates to the bacterial method for nitrate isotopic analyses. *Anal Chem*. 2011;83(5):1850-1856. doi:10.1021/ac1028984
12. Weigand MA, Foriel J, Barnett B, Oleynik S, Sigman DM. Updates to instrumentation and protocols for isotopic analysis of nitrate by the denitrifier method. *Rapid Commun Mass Spectrom*. 2016;30(12):1365-1383. doi:10.1002/rcm.7570
13. Knapp AN, Sigman DM. Stable isotopic composition of dissolved organic nitrogen from the surface waters of the Sargasso Sea. In: *ASLO Annual Meeting, Salt Lake City, Utah*; 2003.
14. Knapp AN, Sigman DM, Lipschultz F. N isotopic composition of dissolved organic nitrogen and nitrate at the Bermuda Atlantic Time-series Study site. *Global Biogeochem Cycles*. 2005;19(1):GB1018. doi:10.1029/2004GB002320
15. Robinson RS, Brunelle BG, Sigman DM. Revisiting nutrient utilization in the glacial Antarctic: evidence from a new method for diatom-bound N isotopic analysis. *Paleoceanography*. 2004;19(3):PA3001. doi:10.1029/2003PA000996
16. Nydahl F. On the peroxodisulphate oxidation of total nitrogen in waters to nitrate. *Water Res*. 1978;12(12):1123-1130. doi:10.1016/0043-1354(78)90060-X
17. Auderset A, Moretti S, Taphorn B, et al. Enhanced ocean oxygenation during Cenozoic warm periods. *Nature*. 2022;609(7925):77-82. doi:10.1038/s41586-022-05017-0
18. Costa KM, McManus JF, Anderson RF, et al. No iron fertilization in the equatorial Pacific Ocean during the last ice age. *Nature*. 2016;529(7587):519-522. doi:10.1038/nature16453
19. Ren H, Sigman DM, Chen MT, et al. Elevated foraminifera-bound nitrogen isotopic composition during the last ice age in the South China Sea and its global and regional implications. *Global Biogeochem Cycles*. 2012;26:GB1031. doi:10.1029/2010GB004020
20. Farmer JR, Pico T, Underwood OM, et al. The Bering Strait was flooded 10,000 years before the Last Glacial Maximum. *Proc Natl Acad Sci*. 2023;120(1):e2206742119. doi:10.1073/pnas.2206742119
21. Farmer JR, Sigman DM, Granger J, et al. Arctic Ocean stratification set by sea level and freshwater inputs since the last ice age. *Nat Geosci*. 2021;14(9):684-689. doi:10.1038/s41561-021-00789-y
22. Hess AV, Auderset A, Rosenthal Y, et al. A well-oxygenated eastern tropical Pacific during the warm Miocene. *Nature*. 2023;619(7970):521-525. doi:10.1038/s41586-023-06104-6
23. Kast ER, Stolper DA, Auderset A, et al. Nitrogen isotope evidence for expanded ocean suboxia in the early Cenozoic. *Science*. 2019;364(6438):386-389. doi:10.1126/science.aau5784
24. Martínez-García A, Sigman DM, Ren H, et al. Iron fertilization of the Subantarctic ocean during the Last Ice Age. *Science*. 2014;343(6177):1347-1350. doi:10.1126/science.1246848
25. Ren H, Sigman DM, Martínez-García A, et al. Impact of glacial/interglacial sea level change on the ocean nitrogen cycle. *PNAS*. 2017;114(33):E6759-E6766. doi:10.1073/pnas.1701315114
26. Ren H, Sigman DM, Meckler AN, et al. Foraminiferal isotope evidence of reduced nitrogen fixation in the Ice Age Atlantic Ocean. *Science*. 2009;323(5911):244-248. doi:10.1126/science.1165787
27. Ren H, Sigman DM, Thunell RC, Prokopenko MG. Nitrogen isotopic composition of planktonic foraminifera from the modern ocean and recent sediments. *Limnol Oceanogr*. 2012;57(4):1011-1024. doi:10.4319/lo.2012.57.4.1011
28. Ren H, Studer AS, Serno S, et al. Glacial-to-interglacial changes in nitrate supply and consumption in the subarctic North Pacific from microfossil-bound N isotopes at two trophic levels. *Paleoceanography*. 2015;30(9):1217-1232. doi:10.1002/2014PA002765
29. Straub M, Sigman DM, Ren H, et al. Changes in North Atlantic nitrogen fixation controlled by ocean circulation. *Nature*. 2013;501(7466):200-203. doi:10.1038/nature12397
30. Straub M, Tremblay MM, Sigman DM, et al. Nutrient conditions in the subpolar North Atlantic during the last glacial period reconstructed from foraminifera-bound nitrogen isotopes. *Paleoceanography*. 2013;28(1):79-90. doi:10.1002/palo.20013
31. Wang XT, Wang Y, Auderset A, et al. Oceanic nutrient rise and the late Miocene inception of Pacific oxygen-deficient zones. *Proc Natl Acad Sci*. 2022;119(45):e2204986119. doi:10.1073/pnas.2204986119
32. DeLong KL, Palmer K, Wagner AJ, et al. The Flower Garden Banks *Siderastrea siderea* coral as a candidate Global boundary Stratotype Section and Point for the Anthropocene series. *Anthr Rev*. 2023;10(1):225-250. doi:10.1177/20530196221147616
33. Duprey NN, Wang TX, Kim T, et al. Megacity development and the demise of coastal coral communities: evidence from coral skeleton δ15N records in the Pearl River estuary. *Glob Chang Biol*. 2020;26(3):1338-1353. doi:10.1111/gcb.14923
34. Duprey NN, Wang XT, Thompson PD, et al. Life and death of a sewage treatment plant recorded in a coral skeleton δ15N record. *Mar Pollut Bull*. 2017;120(1-2):109-116. doi:10.1016/j.marpolbul.2017.04.023
35. Erler DV, Farid HT, Glaze TD, Carlson-Perret NL, Lough JM. Coral skeletons reveal the history of nitrogen cycling in the coastal Great Barrier Reef. *Nat Commun*. 2020;11(1):1500. doi:10.1038/s41467-020-15278-w
36. Erler DV, Nothdurft L, McNeil M, Moras CA. Tracing nitrate sources using the isotopic composition of skeletal-bound organic matter from the calcareous green algae *Halimeda*. *Coral Reefs*. 2018;37(4):1003-1011. doi:10.1007/s00338-018-01742-z
37. Erler DV, Shepherd BO, Linsley BK, Nothdurft LD, Hua Q, Lough JM. Has nitrogen supply to coral reefs in the South Pacific Ocean changed over the past 50 thousand years? *Paleoceanogr Paleoclimatol*. 2019;34(4):567-579. doi:10.1029/2019PA003587
38. Erler DV, Wang XT, Sigman DM, Scheffers SR, Shepherd BO. Controls on the nitrogen isotopic composition of shallow water corals across a tropical reef flat transect. *Coral Reefs*. 2015;34(1):329-338. doi:10.1007/s00338-014-1215-5
39. Muscatine L, Goiran C, Land L, Jaubert J, Cuif J-P, Allemand D. Stable isotopes (δ13C and δ15N) of organic matrix from coral skeleton. *PNAS*. 2005;102(5):1525-1530. doi:10.1073/pnas.0408921102

40. Wang XT, Prokopenko MG, Sigman DM, et al. Isotopic composition of carbonate-bound organic nitrogen in deep-sea scleractinian corals: a new window into past biogeochemical change. *Earth Planet Sci Lett*. 2014;400:243-250. doi:10.1016/j.epsl.2014.05.048
41. Wang XT, Sigman DM, Cohen AL, et al. Influence of open ocean nitrogen supply on the skeletal δ15N of modern shallow-water scleractinian corals. *Earth Planet Sci Lett*. 2016;441:125-132. doi:10.1016/j.epsl.2016.02.032
42. Wang XT, Sigman DM, Cohen AL, et al. Isotopic composition of skeleton-bound organic nitrogen in reef-building symbiotic corals: a new method and proxy evaluation at Bermuda. *Geochim Cosmochim Acta*. 2015;148:179-190. doi:10.1016/j.gca.2014.09.017
43. Wang XT, Sigman DM, Prokopenko MG, et al. Deep-sea coral evidence for lower Southern Ocean surface nitrate concentrations during the last ice age. *PNAS*. 2017;114(13):3352-3357. doi:10.1073/pnas.1615718114
44. Zinke J, Cantin NE, DeLong KL, et al. North Flinders Reef (Coral Sea, Australia) *Porites* sp. corals as a candidate Global boundary Stratotype Section and Point for the Anthropocene series. *Anthr Rev*. 2023;10(1):201-224. doi:10.1177/20530196221142963
45. Kast ER, Griffiths ML, Kim SL, et al. Cenozoic megatooth sharks occupied extremely high trophic positions. *Sci Adv*. 2022;8(25):eabl6529. doi:10.1126/sciadv.abl6529
46. Leichliter JN, Lüdecke T, Foreman AD, et al. Tooth enamel nitrogen isotope composition records trophic position: a tool for reconstructing food webs. *Commun Biol*. 2023;6(1):1, 373-13. doi:10.1038/s42003-023-04744-y
47. Leichliter JN, Lüdecke T, Foreman AD, et al. Nitrogen isotopes in tooth enamel record diet and trophic level enrichment: results from a controlled feeding experiment. *Chem Geol*. 2021;563:120047. doi:10.1016/j.chemgeo.2020.120047
48. Lüdecke T, Leichliter JN, Aldeias V, et al. Carbon, nitrogen, and oxygen stable isotopes in modern tooth enamel: a case study from Gorongosa National Park, central Mozambique. *Front Ecol Evol*. 2022;10. doi:10.3389/fevo.2022.958032
49. Lueders-Dumont JA, Forden AG, Kast ER, et al. Controls on the nitrogen isotopic composition of fish otolith organic matter: lessons from a controlled diet switch experiment. *Geochim Cosmochim Acta*. 2022;316:69-86. doi:10.1016/j.gca.2021.09.030
50. Lueders-Dumont JA, Sigman DM, Johnson BJ, Jensen OP, Oleynik S, Ward BB. Comparison of the isotopic composition of fish otolith-bound organic N with host tissue. *Can J Fish Aquat Sci*. 2020;77(2):264-275. doi:10.1139/cjfas-2018-0360
51. Lueders-Dumont JA, Wang XT, Jensen OP, Sigman DM, Ward BB. Nitrogen isotopic analysis of carbonate-bound organic matter in modern and fossil fish otoliths. *Geochim Cosmochim Acta*. 2018;224:200-222. doi:10.1016/j.gca.2018.01.001
52. Ai XE, Studer AS, Sigman DM, et al. Southern Ocean upwelling, Earth's obliquity, and glacial-interglacial atmospheric CO_2 change. *Science*. 2020;370(6522):1348-1352. doi:10.1126/science.abd2115
53. Brunelle BG, Sigman DM, Cook MS, et al. Evidence from diatom-bound nitrogen isotopes for subarctic Pacific stratification during the last ice age and a link to North Pacific denitrification changes. *Paleoceanography*. 2007;22(1). doi:10.1029/2005PA001205
54. Robinson RS, Sigman DM. Nitrogen isotopic evidence for a poleward decrease in surface nitrate within the Ice Age Antarctic. *Quat Sci Rev*. 2008;27(9-10):1076-1090. doi:10.1016/j.quascirev.2008.02.005
55. Robinson RS, Sigman DM, DiFiore PJ, Rohde MM, Mashiotta TA, Lea DW. Diatom-bound $^{15}N/^{14}N$: new support for enhanced nutrient consumption in the Ice Age subantarctic. *Paleoceanography*. 2005;20(3):PA3003. doi:10.1029/2004PA001114
56. Studer AS, Ellis KK, Oleynik S, Sigman DM, Haug GH. Size-specific opal-bound nitrogen isotope measurements in North Pacific sediments. *Geochim Cosmochim Acta*. 2013;120:179-194. doi:10.1016/j.gca.2013.06.041
57. Studer AS, Martínez-Garcia A, Jaccard SL, Girault FE, Sigman DM, Haug GH. Enhanced stratification and seasonality in the Subarctic Pacific upon Northern Hemisphere Glaciation—new evidence from diatom-bound nitrogen isotopes, alkenones and archaeal tetraethers. *Earth Planet Sci Lett*. 2012;351–352:84-94. doi:10.1016/j.epsl.2012.07.029
58. Studer AS, Sigman DM, Martínez-García A, et al. Antarctic Zone nutrient conditions during the last two glacial cycles. *Paleoceanography*. 2015;30:2014PA002745. doi:10.1002/2014PA002745
59. Studer AS, Sigman DM, Martínez-García A, et al. Increased nutrient supply to the Southern Ocean during the Holocene and its implications for the pre-industrial atmospheric CO_2 rise. *Nature Geosci*. 2018;11(10):756-760. doi:10.1038/s41561-018-0191-8
60. Bodelier PLE, Wijlhuizen AG, Blom CWPM, Laanbroek HJ. Effects of photoperiod on growth of and denitrification by *Pseudomonas chlororaphis* in the root zone of *Glyceria maxima*, studied in a gnotobiotic microcosm. *Plant and Soil*. 1997;190:91-103. doi:10.1023/A:1004212814097
61. Sigman DM, DiFiore PJ, Hain MP, et al. The dual isotopes of deep nitrate as a constraint on the cycle and budget of oceanic fixed nitrogen. *Deep-Sea Res I Oceanogr Res Pap*. 2009;56(9):1419-1439. doi:10.1016/j.dsr.2009.04.007
62. Martínez-García A, Jung J, Ai XE, et al. Laboratory assessment of the impact of chemical oxidation, mineral dissolution, and heating on the nitrogen isotopic composition of fossil-bound organic matter. *Geochem Geophys Geosyst*. 2022;23:e2022GC010396. doi:10.1029/2022GC010396
63. Sigman DM, Altabet MA, Francois R, McCorkle DC, Gaillard J-F. The isotopic composition of diatom-bound nitrogen in Southern Ocean sediments. *Paleoceanography*. 1999;14(2):118-134. doi:10.1029/1998PA900018
64. Wang, X.T., 2016. *Nitrogen isotopes in scleractinian corals: modern ocean studies and paleoceanographic applications*. Dissertation. Princeton University.
65. Von Euw S, Zhang Q, Manichev V, et al. Biological control of aragonite formation in stony corals. *Science*. 2017;356(6341):933-938. doi:10.1126/science.aam6371
66. Yoshioka S, Kitano Y. Transformation of aragonite to calcite through heating. *Geochem J*. 1985;19(4):245-249. doi:10.2343/geochemj.19.245
67. John E, Stephan D. Calcium silicate hydrate—in-situ development of the silicate structure followed by infrared spectroscopy. *J Am Ceram Soc*. 2021;104(12):6611-6624. doi:10.1111/jace.18019
68. Greenberg SA. Reaction between silica and calcium hydroxide solutions. I. Kinetics in the temperature range 30 to 85°[1]. *J Phys Chem*. 1961;65(1):12-16. doi:10.1021/j100819a005
69. Studer AS, Mekik F, Ren H, et al. Ice Age-Holocene similarity of foraminifera-bound nitrogen isotope ratios in the eastern equatorial Pacific. *Paleoceanogr Paleoclimatol*. 2021;36:e2020PA004063. doi:10.1029/2020PA004063

SUPPORTING INFORMATION

Additional supporting information can be found online in the Supporting Information section at the end of this article.

How to cite this article: Moretti S, Duprey NN, Foreman AD, et al. Analytical improvements and assessment of long-term performance of the oxidation–denitrifier method. *Rapid Commun Mass Spectrom*. 2024;38(1):e9650. doi:10.1002/rcm.9650